Journal of Fluids and Structures 69 (2017) 187–208

Contents lists available at ScienceDirect

Journal of Fluids and Structures

journal homepage: www.elsevier.com/locate/jfs

Measurement and modeling of lift enhancement on plunging airfoils: A frequency response approach

M.Y. Zakaria[a,*], H.E. Taha[b], M.R. Hajj[a]

[a] Virginia Tech, Blacksburg, VA 24061, USA
[b] University of California, Irvine, CA 92697, USA

ARTICLE INFO

Keywords:
Unsteady aerodynamics
Lift enhancement
Frequency response
High angles of attack
Leading edge vortex

ABSTRACT

A frequency response approach is taken to model unsteady aerodynamics resulting from plunging oscillations of an airfoil. The oscillations range covers high angles of attack (up to 65°) and reduced frequencies (up to 0.95) with particular attention to the range of flow nonlinearities over which lift enhancement is observed. Experiments were performed in a wind tunnel on an airfoil section at a Reynolds number of 80,000. Airfoil acceleration and lift force data were used to determine the frequency response functions between the measured unsteady lift and the quasi-steady lift. The results show enhanced lift amplitude over the stall regime at a reduced frequency of 0.7. The flow dynamics associated with this observation were identified from water tunnel experiments. Particular attention is paid to the flow separation and consequent formation and convection of the leading edge vortex. An optimization-based system identification approach is performed to represent the unsteady lift by a fourth-order dynamical system. This representation is suitable for sensitivity, dynamics and control analyses especially for applications where unsteady aerodynamics can be exploited for the purpose of lift enhancement.

1. Introduction

Modeling of unsteady aerodynamics has continued to receive attention since the early theoretical foundations of Prandtl (1924) and Birnbaum (1924). Over this period, two main constructive approaches can be distinguished. The first approach, laid down by Prandtl more than 90 years ago, is to assume that continuous sheets of vorticity emanate from the body's “sharp” edges and that the flow outside of these sheets can be modeled using inviscid assumptions. This approach has been the cornerstone of many analytical and efficient numerical unsteady aerodynamic models for bio-inspired flight (Zakaria et al., 2015b) and prediction of flutter boundaries (Zakaria et al., 2015a). The other approach is based on direct simulation of the governing Navier-Stokes equations with proper spatial and temporal discretization algorithms. Although the latter approach provides high-fidelity detailed descriptions of the flow field, it lacks efficiency and stipulates too high of a computational burden to be used in design optimization, analysis of fluid-body-dynamics interactions, or even in studying the nonlinear dynamical characteristics of the flow field per se. On the other hand, Prandtl's approach is much more efficient and may, sometimes, lead to representations that are very convenient to some applications. Yet, it is quite limited to linearized, attached, potential flow cases and can hardly be extended to the recent interesting applications that invoke and exploit unsteady flow separation.

The increased interest in biologically-inspired flights has created a substantial research activity in unsteady aerodynamics of low

* Corresponding author.
E-mail address: zakaria@vt.edu (M.Y. Zakaria).

http://dx.doi.org/10.1016/j.jfluidstructs.2016.12.004
Received 14 April 2016; Received in revised form 23 November 2016; Accepted 2 December 2016
Available online 04 January 2017
0889-9746/ Published by Elsevier Ltd.

Nomenclature

c	Airfoil chord $2b$ (m)
C_L	Lift coefficient
e	Error between measured and optimized values
f	Frequency (Hz)
G	Transfer function
h_a	Plunging amplitude
h_{tunnel}	Wing model height from ground, (m)
k	Reduced frequency $\pi fc/U_\infty$
ℓ	Wing span (m)
p	Non-dimensional Laplace variable
q	Dynamic pressure, $\rho U_\infty^2/2$
Re	Reynolds number, $\rho U_\infty c/\mu$
T	Time period
U_∞	Free stream velocity, (m/s)

Greek

α_o	Airfoil mean angle of attack
α_{eff}	Effective angle of attack
ω	Frequency of oscillation, (rad/s)
ρ	Air density, (kg/m^3)

Subscripts

a	Amplitude
s	Quasi-steady
c	Circulatory

Acronyms

AoA	Angle of attack
LEV	Leading edge vortex
TEV	Trailing edge vortex

Reynolds number (*Re*) flyers. Two main aspects have been found to characterize this range of low *Re* flight: (i) the almost no sharp stall with a smooth lift variation over a broad range of angles of attack and (ii) the presence of a stabilized leading edge vortex (LEV) that enhances lift characteristics of such flights, see Dickinson and Gotz (1993), Ellington et al. (1996b), Dickinson et al. (1999). In addition, the experimental study of Dickinson et al. (1999) and the computational results of Ramamurti and Sandberg (2002) indicate that the shear force contribution to the aerodynamic loads is minimal.

Theoretical studies :. The above characteristics of low *Re* flows have been modeled by extending Prandtl's classical theory of unsteady aerodynamics to biologically-inspired flows. Saffman and Sheffield (1977) were the first to attribute the enhancement in mean lift to an attached LEV; a concept that has since been supported by several investigations including the recent work of Li and Wu (2015). One simple extension to Prandtl's classical theory, proposed by Minotti (2002), is to add a stationary vortex with respect to the airfoil to account for the LEV effects. Minotti (2002) also determined the optimum location of this vortex to match the experimental results of Dickinson et al. (1999). Jones (2003) developed a potential flow model for the unsteady separation by shedding continuous sheets of vorticity from both the leading and trailing edges. His use of the Rott-Birkhoff equation that describes the evolution of free sheets of vorticity in potential flows along with the mathematical rigor of his formulation allowed implicit satisfaction of the Kutta condition at both edges by imposing boundedness of the flow velocity everywhere. However, the numerical implementation was cumbersome and even diverged for cases where the simulated maneuver incorporated both low and high angles of attack. Similar approaches were proposed by Yongliang et al. (2003), Pullin and Wang (2004) and Ansari et al. (2006). Ramesh et al. (2014) developed a new LEV shedding criterion. They used the A_0 coefficient in the Fourier series of the bound circulation distribution to serve as a criterion for predicting the onset of flow separation at the leading edge and called it the Leading Edge Suction Parameter (LESP). They showed that there is a critical value of the LESP (depending on airfoil shape and *Re*) that determines whether the flow is attached or separated at the leading edge, irrespective of the motion kinematics. Their LESP criterion not only predicts the onset and termination of LEV shedding but also the strength of the newly shed LEV without a need to invoke the Kutta condition. This work was extended by Ramesh et al. (2015) to study limit cycle oscillations of airfoils operating at low *Re*. The authors concluded that the aerodynamic nonlinearities produced by intermittent LEV shedding may cause a supercritical-Hopf bifurcation.

V. OL et al. (2009) and Wang and Eldredge (2012) proposed a remedy for the high computational cost associated with continuous vorticity shedding from both edges as applied by Ansari et al. (2006). Instead of shedding constant-strength point vortices at each time step from both leading and trailing edges, they shed variable-strength point vortices at larger time lapses. This formulation greatly reduced the number of degrees of freedom and enhanced the efficiency of the discrete vortex model. However, they determined the strength of the free vortices at each time step by satisfying the Kutta condition at both edges, which is questionable in these highly unsteady applications, as shown by Pitt Ford and Babinsky (2013), Savage et al. (1979) and invoked by Ansari et al. (2006). Hemati et al. (2014) improved their varying-strength discrete vortex model by relaxing the Kutta condition and using optimal control theory to determine a law that governs the rate of change of vortex strength (i.e., instead of the Kutta condition) to minimize the discrepancy between predicted and measured forces. Their development of a compact dynamical model that governs such an unsteady flow allowed for the use of optimal control theory to better understand the flow dynamics, and more specifically, to construct the flow field from only force measurements. Brunton and Rowley (2013) extended Theodorsen's model of the lift frequency response Theodorsen (1935) to low *Re* flows.

Taha et al. (2014) proposed a simple extension to the classical unsteady formulation. In particular, they extended Duhamel's superposition principle, commonly used in unsteady linear aerodynamics, to arbitrary unconventional lift mechanisms with emphasis on capturing the dominant nonlinear effects of LEV in insect flight. They proposed the quasi-steady circulation as the appropriate aerodynamic input that should be used in convolution with the Wagner's step response (Wagner, 1925) in the Duhamel's principle. Then, they constructed a state space formulation for the developed model and validated it against results from

direct numerical simulations by Sun and Du (2003) on the wings of several hovering insects. The model of Taha et al. (2014) captures the nonlinearity of the input-output map but its underpinning flow dynamics is the Wagner's linear response. In order to capture the nonlinearity of the lift evolution dynamics, Yan et al. (2014) and Taha et al. (2015) revisited the classical work of Theodorsen (1935) and relaxed four of its major assumptions (1) flat wake, (2) small angle of attack, (3) small disturbances to the mean flow components, and (4) time-invariant free-stream. They developed a semi-analytical model that is more efficient than classical discrete vortex models and can be applied successfully to large amplitude maneuvers. They simulated a large-amplitude canonical pitch maneuver, introduced by Eldredge et al. (2009), and compared the obtained results with the computational results and experimental data of Ramesh et al. (2013) and the classical unsteady model of Leishman and Nguyen (1990). The classical unsteady results deviated considerably from the experimental and computational results at large angles of attack. On the other hand, the reduced-order model developed by Yan et al. (2014) produced satisfactory results for the generated lift and thus covered a gap in the classical theory of unsteady aerodynamics. Based on this model, Taha et al. (2015) showed that the frequency response, and consequently the flow dynamics, change considerably as the angle of attack increases. In particular, they showed a large departure from Theodorsen's model in the amplitude and phase for airfoils oscillating around 40° angle of attack. This finding shows the need for developing and validating unsteady aerodynamics models that cover high angles of attack and high reduced frequencies.

Experimental studies :. In addition to the above theoretical developments, there have been several experimental investigations to study the effects of the wake structure on lift augmentation and attenuation at various reduced frequencies for pitching, plunging and surging motions, e.g., the work of Ellington et al. (1996a) and Jones et al. (1996). The work of Commerford and Carta (1974) is one of the earliest experimental investigations of the lift response due to high frequency flow fluctuations. They placed an airfoil in the natural wake shed behind a cylinder at low Reynolds number (i.e., in the Von Karman street). The authors showed enhancement in lift amplitude over potential flow theoretical predictions for angles of attack up to 20° at a reduced frequency k=3.9. An optimal range of Strouhal number ($0.25 \leq S_t \leq 0.35$) over which an enhanced mean thrust and/or mean lift is observed was also found by several authors including Triantafyllou et al. (1993), Anderson et al. (1998), Ohmi et al. (1991), Wang (2005) and Cleaver et al. (2012). Most of these studies however, covered the relatively low angles of attack. It should be noted that there have been two types of observed lift enhancement in literature: (i) enhancement in the generated mean lift force and (ii) enhancement in the lift amplitude. The mean type will be useful for design considerations where a specific mean lift force is typically required. However, the amplitude type will be useful in dynamics applications where the unsteady lift dynamics affects performance.

Rival and Tropea (2010) experimentally investigated the mean lift augmentation and the associated unfavorable pitching moment due to dynamic stall. They elucidated the gradual transition from a bluff-body-type (multiple vortex pairs) to a mushroom-type wake at a reduced frequency k=0.2. In order to have a better insight into the flow dynamics that leads to such a lift enhancement, Rival et al. (2014) conducted direct-force and velocity-field measurements to analyze the development and reattachment of the LEVs from a plunging airfoil at Re=10, 000 and k=0.25, for three different leading-edge geometries. The leading-edge shape was shown to have a direct effect on the shear layer that forms the LEV, and consequently on the development of the LEV, which we find to be contradicting to the conclusions of Usherwood and Ellington (2002) at Re=8000. Panah and Buchholz (2014) found out that the LEV circulation is highly sensitive to the Strouhal number in the range $0.3 < S_t < 0.5$. Baik et al. (2012) studied the flow evolution and unsteady force generation over pitching and plunging airfoils about some mean angle of attack and concluded that the Strouhal number is the most important parameter controlling the LEV maximum strength and the aerodynamic force generation.

Heathcote and Gursul (2007) described two lift enhancement mechanisms for plunging airfoils: deflected jets and convected LEVs. Stable deflected jets form at high Strouhal numbers and pre-stall conditions. Deflected jets are caused by pairing of the clockwise and counter-clockwise trailing-edge-vortices (TEVs) to form dipoles. These dipoles are asymmetric in position and strength, and therefore self-advect at an inclined direction to the free stream creating pressure difference in the flow field (flow asymmetry). This asymmetry results in high lift coefficients, even for a zero degree angle of attack. Deflected jets do not form at low Strouhal numbers due to insufficient vortex strength, nor at larger incidences due to forcing in a particular direction. Convected LEVs were determined to be an effective means for lift enhancement at post-stall angles of attack. At low Strouhal numbers, a LEV forms on the upper surface of the airfoil during the downward motion of the airfoil and then convects creating a low pressure region. As these LEVs are created by the plunging motion, the increase in lift coefficient is approximately proportional to the plunge velocity. Gursul et al. (2014) concluded that this form of flow control is particularly effective when the plunging frequency equals the natural shedding frequency, its harmonics or sub-harmonics.

Pitt Ford and Babinsky (2013) performed an experiment on an impulsively started flat plate at Re=30, 000 and angle of attack $\alpha = 15°$ to study the LEV build-up. They developed a potential flow model that consisted of a bound circulation, free LEVs and free TEVs. They determined the locations and strengths of the LEVs and TEVs using the γ_2-method (Graftieaux et al., 2001) applied to PIV measurements. As such, they could determine the value of the bound circulation in the potential flow model that results in minimum deviation between the potential flow field and PIV measurements. Interestingly, during early stages, the optimum bound circulation was found to be Kelvin's value obtained by satisfying Kelvin's law of zero total circulation, i.e., conservation of angular momentum in inviscid flows, which is considerably different from the Kutta's value obtained by satisfying the Kutta condition at the trailing edge. However, during later stages, the Kutta's value is closer to the optimum bound circulation than Kelvin's.

Objectives :. Despite the above advances, there is a need for unsteady nonlinear aerodynamic models that are (i) efficient enough to be used in optimization and control and (ii) rich enough to capture nonlinearity of the flow dynamics and potential lift enhancement mechanisms. In this effort, we conduct static and dynamic plunging-oscillation experiments on a two-dimensional NACA-0012 airfoil at Re=79,900 in the range of reduced frequencies $0.15 \leq k \leq 0.95$ and mean angles of attack α_0 between 0° and 65°. Spectral analysis is then performed to evaluate the frequency content of fluctuations at different angles of attack and flow

regimes. The unsteady loads were measured at different frequencies. We use these measurements to calculate mean values of the generated circulated lift. Additionally, we construct the frequency response between the plunging motion represented by its quasi-steady lift (static lift data integrated with the effective angle of attack) as an input and the unsteady lift as an output in the pre-stall, stall and post-stall regimes. We also use these measurements to identify and model the flow dynamics associated with increase in lift amplitude. Then, we perform an optimization-based system identification to represent the unsteady lift by a finite dimensional dynamical system for each constructed frequency response. As such, we assess the effects of the mean angle of attack on lift build-up dynamics. In addition, we perform flow visualization experiments at different reduced frequencies to gain insight into the physical concepts underpinning the lift enhancement mechanism and the associated LEV dynamics.

2. Experimental setup

2.1. Wind tunnel facility and operating conditions

The experiments were conducted in an open-jet-return, low-speed wind tunnel. The test chamber has a cross section of 0.7 m×0.7 m and a length of 1.5 m. The maximum attainable air speed is 28 m/s. The operated flow speed for the current experiments is 8.6 m/s $\pm 0.5\%$. The tunnel free stream turbulence intensity is 1% at $U_\infty = 8.6$ m/s, which corresponds to a chord Reynolds number of 79,900. The flow speed is controlled by an $AF600$ General Electric variable frequency drive. The test rig mainly consists of an oscillatory driving motor and a set of linkages connected together with a tunnel-spanning profile. The mechanism is able to perform pitch, plunge and combined motions at high setting angles of attack. The key component is the driving oscillatory rod that is connected to two threaded rear push-rod used to change the mean angle of attack of the wing. An adjustment nut is fitted along with each push-rod to allow for varying the mean angle of attack, α_0, between 0° and 65°. The motor has an operating frequency in the range of $0\ Hz < f_{motor} < 50$ Hz at no load conditions with a constant full stroke length h_o=1.93 cm. The main oscillatory rod is attached to a small bracket which, in turn, is attached to the mid-span wing profile at the quarter chord location. The two push-rods are attached upside down to the profile at the three quarter chord location. To achieve pure plunging motion, the push-rods are attached to the main oscillatory rod at the required mean angle of attack α_0, as shown in Fig. 1. A foam core NACA 0012 was machined using a laser cutter and reinforced with a carbon fiber rod of diameter 4 mm at quarter chord location and the whole profile was covered by two layers of carbon fiber fabric to guarantee rigidity in span-wise direction. The carbon-fiber wing has an aspect ratio of 4.5 with a chord length of 0.14 m and a span of 0.63 m. The wing model was mounted horizontally in the center of the test section. We use end plates (each plate is 0.25 m long and 0.15 m wide) to ensure two-dimensional flow within 2.7%. Wind tunnel blockage was less than 3.7% when the airfoil was set at the maximum angle of attack.

2.2. Force balance and data processing

The wind tunnel is equipped with a six component strain gauge balance of strut model support system having an accuracy of 1.2% (0.05 N). The data were collected and processed using a sampling frequency rate of 2500 Hz. The measured signals were amplified by a transducer amplifier and connected to a National Instruments SCXI 1520 Multifunction DAQ. Force measurements were ensemble-averaged over three experiments and force coefficients were evaluated in terms of the dynamic pressure corresponding to the steady-state velocity, U_∞, rather than the instantaneous velocity. The wing oscillatory motion was measured using MEMS accelerometers. Two accelerometers were used for redundancy. A third accelerometer was placed on the strut balance base bracket to ensure that the vibrational structural response of the balance has negligible effects, i.e., the natural frequency of the balance is away from the operating frequency. The accelerometers were calibrated using a 2 MHz variable phase synthesizer apparatus at different operating frequencies with an uncertainty of 0.5% over the range of operating conditions. The motion was captured using both accelerometers. The data was filtered using a digital fourth order butterworth low pass filter with a cut-off frequency of 50 Hz, which is considerably higher than the maximum excitation frequency (17.6 Hz). Fig. 2(a) shows the actual plunging motion, obtained by integrating the mean acceleration of the two accelerometers, versus an ideal sin wave having the same frequency, amplitude and phase. Fig. 2(b) shows the power spectrum of the accelerometer's signals; a clear distinct peak indicating

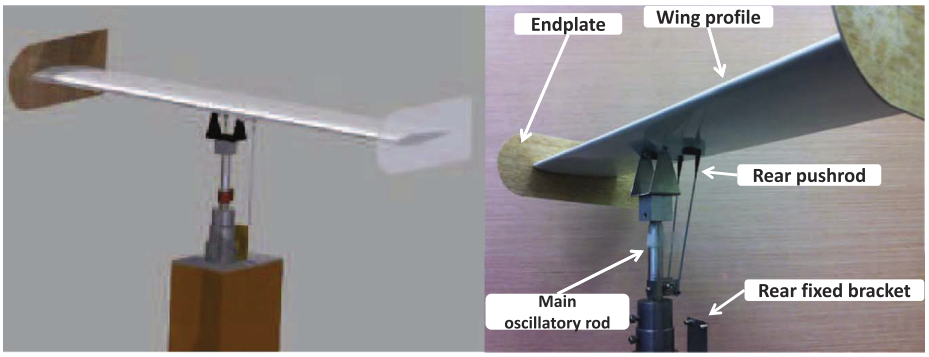

Fig. 1. Three dimensional views of the pitch-plunge mechanism.

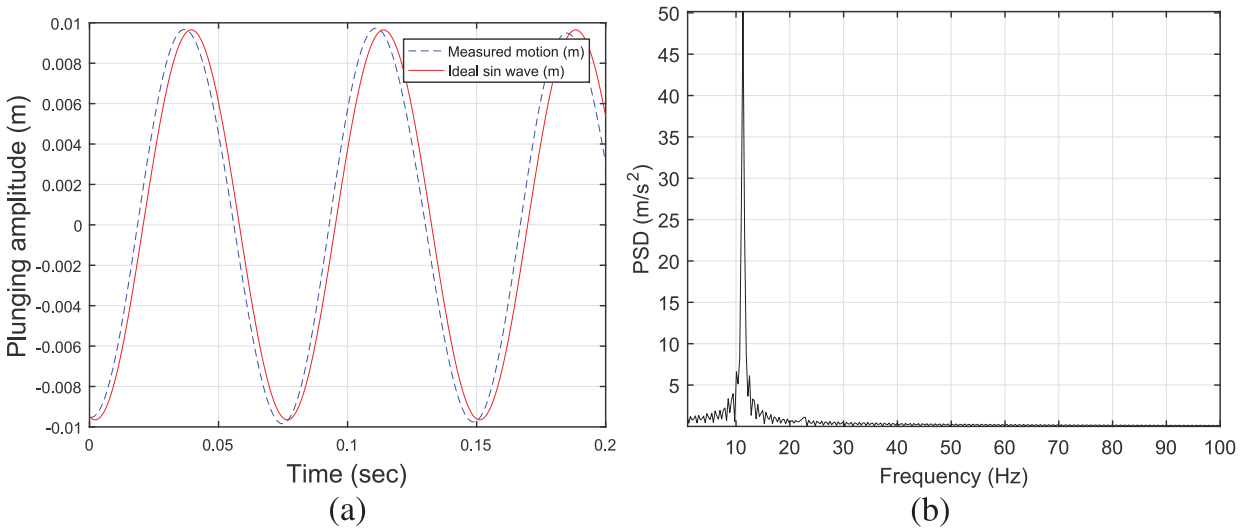

Fig. 2. (a) Actual plunging displacement compared to a corresponding ideal sine wave and (b) actual acceleration power spectrum for the case of $\alpha_o = 0$ and k=0.57.

one frequency content. A digital protractor was used to measure the wing setting angle with an error of $\pm 0.2°$. The frequency of the wing was also verified using a non-contact type optical, digital tachometer. Fig. 3 shows the whole setup of the pitch-plunge mechanism and the tunnel facility.

2.3. Wind tunnel corrections

A common problem associated with open-jet wind tunnels is the induced pressure fluctuations in the test section. These fluctuations can limit the effective wind speed range. These fluctuations are normally attributed to a coupling between large scale coherent vortices shed from the nozzle and wind tunnel resonant modes. To determine the mean velocity at different locations, time series were measured at different positions along the spanwise direction in the presence of the wing. In addition, the vibration of the test stand from its interaction with the flow field was measured. Furthermore, the uniformity of the flow field at the nozzle outlet was assessed using a traverse system attached with a pitot tube to measure the pressure along a line perpendicular to the flow direction. Based on all of the above flow characterizations, the airfoil section was mounted at 1.48 m from the tunnel floor and 0.25 m from the nozzle outlet.

In an effort to identify the pressure fluctuations in the open-jet wind tunnel, an analytical scheme proposed by Brooks et al. (1984) was used to calculate the effective angle of attack due to open-jet wind tunnel corrections. It should be noted that, since the flow is free to expand, the effects of solid and wake blockages are typically neglected for open jet flows (Rae and Pope, 1984), as well as the influence of horizontal buoyancy (drop in static pressure along the test section). For an open jet flow, the remaining two corrections, downwash and streamline curvature, have a significant effect on the lift coefficient, C_L, the drag coefficient, C_D and the moment coefficient, C_M. The downwash correction is not needed when two-dimensional testing is carried out with an airfoil section that spans the tunnel width. However, in the present case, the width of the open jet exceeds the span of the airfoil by 3.5 cm. To ensure two dimensionality, end plates were used. The actual size of the end plates was taken into account in the corrections by applying the analytical method proposed by Mangler (1938). The streamline correction accounts for the free divergence of the flow from its original direction downstream of the airfoil section. In open jets, this effect is considerable because there are no tunnel walls

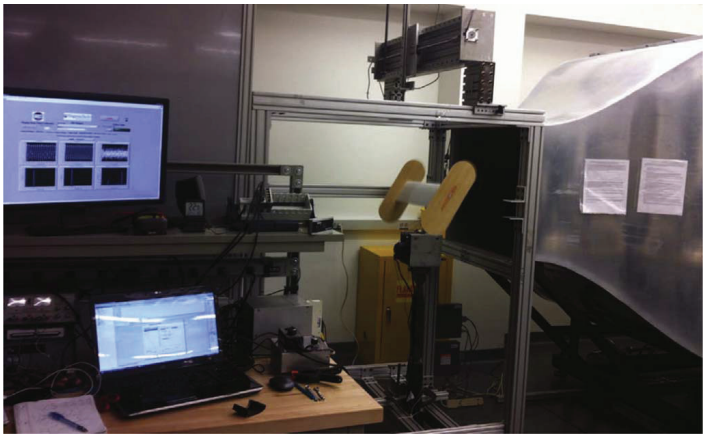

Fig. 3. Experimental setup of the pitch-plunge mechanism in the wind tunnel facility.

to constrain the jet flow. The tunnel flow curvature induces more drag and changes the effective angle of attack. As a result, the measured C_D is larger and the slope of the C_L curve is smaller. Two analytical methods from Garner et al. (1966) and Brooks et al. (1984) that make use of the method of images could be used to correct for these effects. Brook's method involves additional terms for the angle of attack and pitching moment corrections, which indicates that Brook's method is of higher accuracy in comparison to Garner's method and, as such, is used in this work. The flow effective angle of attack, α_{eff}, is then given by:

$$\alpha_{\text{eff}} = \alpha_t - \frac{\sqrt{3\sigma}}{\pi} C_{Lt} - \frac{2\sigma}{\pi} C_{Lt} - \frac{4\sigma}{\pi} C_{Mt} \quad (rad) \tag{1}$$

where α_t is the setting angle of attack, C_{Lt} is the measured lift coefficient, C_{Mt} is the measured pitching moment coefficient, and the nondimensional parameter σ is defined as

$$\sigma = \frac{\pi^2}{48}\left(\frac{c}{h_{\text{tunnel}}}\right)^2$$

where $h_{\text{tunnel}} = 0.7$ m is the wing vertical distance to the ground. Finally, a data reduction program was written to calculate the uncertainties based on Moffat (1985) method considering both bias and precision errors. The results are presented in (Table 1). Eventually, the uncertainty quantification for the operating Reynolds number (Re) is $\pm 2.4\%$, reduced frequency (k) is $\pm 0.24\%$ and static lift coefficient (C_L) is ± 0.05 within the respective ranges operation of 79,900, 0.15–0.95 and 0–1. Uncertainty limits are presented as error bars for each of the dynamic measurements based on three separate runs.

3. Static measurements

3.1. Steady lift curve

As a first step, we measured the static lift curve and compared it to data available in the literature. Fig. 4(a) and 4(b) show respectively the static lift and drag coefficients variation with the angle of attack. The work presented here did not address the dynamic stall behavior and as such, the pitching moment curve is not presented and would be the subject of future work. Fig. 4(a) shows a comparison among the current measurements of the static lift curve at Re=79, 900, the measurements of Tang and Dowell (2014) at Re=313, 000, and theoretical predictions. These predictions include the classical airfoil theory $C_L = 2\pi \sin\alpha$, the potential flow lift without leading edge suction $C_L = 2\pi \sin\alpha \cos^2\alpha$ (Polhamus, 1966), and the fit of the static lift due to a stabilized leading edge vortex $C_L = \pi \sin 2\alpha$, proposed by Berman and Wang (2007) and refined by Taha et al. (2014). Based on standard statistical evaluation methods (assuming Gaussian distribution of data), uncertainty limits with a 95% confidence level are determined for each of the load measurements based on three separate runs. The plots show that the current experimental measurements are in a qualitative agreement with the measurements of Tang and Dowell (2014). Both measurements match predictions of the classical wing theory over its range of applicability (up to 10°). The slight difference in the maximum lift between the current measurements and that of Tang and Dowell (2014) may be attributed to the difference in the Reynolds number and/or blockage effects associated with the closed section in their experiment. As typical for a purely two-dimensional flow, a stabilized leading edge vortex that augments the lift cannot be realized at static conditions. As such, the predictions of the lift due to a stabilized leading edge vortex are higher than the current measurements. Finally, the potential flow model without leading edge suction overestimates the generated lift as it ignores the separation effects. Fig. 4(b) shows that the static drag coefficients increases significantly from values near 0.05 for angles of attack that are smaller than 10° to values above 1 for angles of attack between 50° and 70°.

4. Dynamic measurements and frequency response

In order to asses the frequency response function of a dynamical system, it is important to define the input and output values. Similar to Theodorsen's representation (Theodorsen, 1935), we construct the frequency response between the quasi-steady lift as an aerodynamic input and the circulatory lift as an aerodynamic output. This is also in accordance with the assumption of Taha et al. (2014) that the nonlinearity of lift build-up dynamics may be absorbed in the nonlinear input-output map between the quasi-steady lift and the angle of attack, while the lift dynamics due to changes in the quasi-steady lift may still be considered linear. A supporting finding for this assumption was presented by Pitt Ford and Babinsky (2013). They showed that adding the Wagner's lift (Wagner, 1925) to the non-circulatory contributions obtained using potential flow closely matches the measured lift forces near stall. In the current study, the quasi steady lift is determined from the static lift curve using the instantaneous effective angle of attack, α_{eff}. At each mean angle of attack α_0, the plunging motion is performed such that the variation of the effective angle of attack from its mean

Table 1
Uncertainties of experimental parameters.

Parameter	Range	Uncertainty
Re	79,900	$\pm 2.4\%$
k	0.15–0.95	$\pm 0.24\%$
C_L	0–1	± 0.05

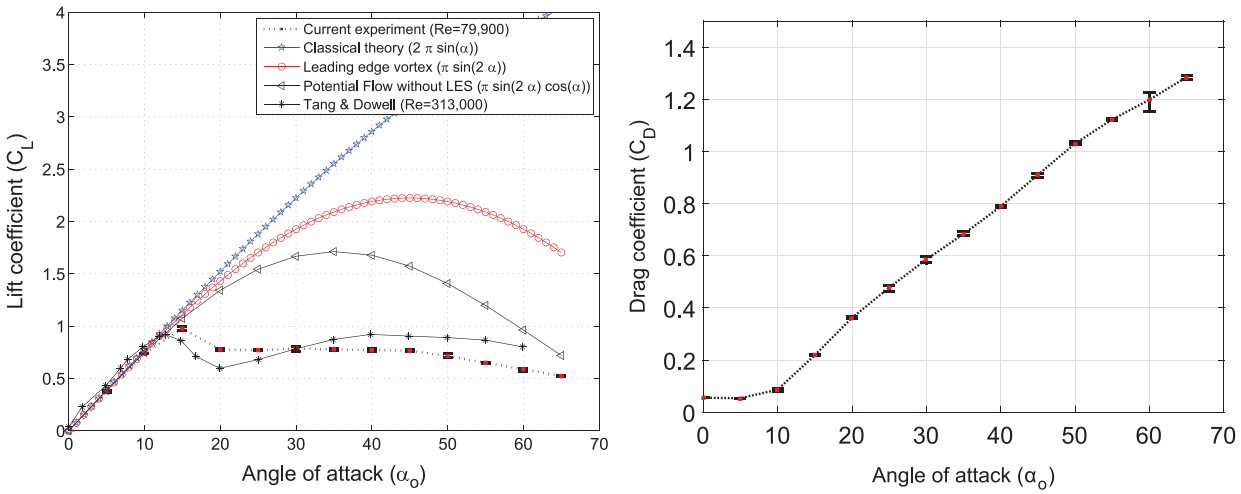

(a) Comparison of the current steady C_L-measurements with theory and other experimental results.

(b) Drag coefficient versus angle of attack.

Fig. 4. Variation of static lift and drag coefficients with angle of attack at *Re*=79,900 for NACA 0012.

value is within a small range. The plunging oscillations, $h(t) = h_a \sin(2\pi ft)$, are performed at various reduced frequencies ($0.15 \leq k \leq 0.95$). It should be noted that due to the use of a semi-automatic speed control (i.e., no feedback regulation), the operating frequencies are not uniformly distributed. By changing the effective angle of attack during the plunging motion, vortices are shed from the leading and trailing edges of the airfoil. The interaction of the shed vortices with the airfoil motion and the shed wake results in a time lag between the airfoil motion and the corresponding aerodynamic load. The frequency response function is a very common means for representing this dynamical behavior. It is commonly known that the frequency response of a given dynamical system is represented by variations of the magnitude and phase of the response function (transfer function) with frequency.

The magnitude variation is important to assess quantities such as lift enhancement and can be used to reconstruct the transfer function. In this work, we use the magnitude of the frequency response function as a measure of the lift enhancement that can be obtained through plunging oscillations of the airfoil. For each combination of mean angle of attack α_0 and reduced frequency k, we define this magnitude as:

$$|G(k;\alpha_0)| = \frac{|C_{L_c}(t;k,\alpha_0)|}{|C_{L_s}(t;k,\alpha_0)|} \tag{2}$$

where $|.|$ denotes the amplitude of the periodic signal, C_{Lc} is the circulatory lift coefficient obtained from the measured lift by subtracting the added mass and inertial effects. The extraction of this component from the measured lift is performed according to:

$$C_{L_c}(t) = [L(t) - (m_{\text{moving}} + \pi\rho\ell b^2\cos^2\alpha)\,\ddot{h}(t)]/\left[\frac{1}{2}\rho U_\infty^2 c\right] \tag{3}$$

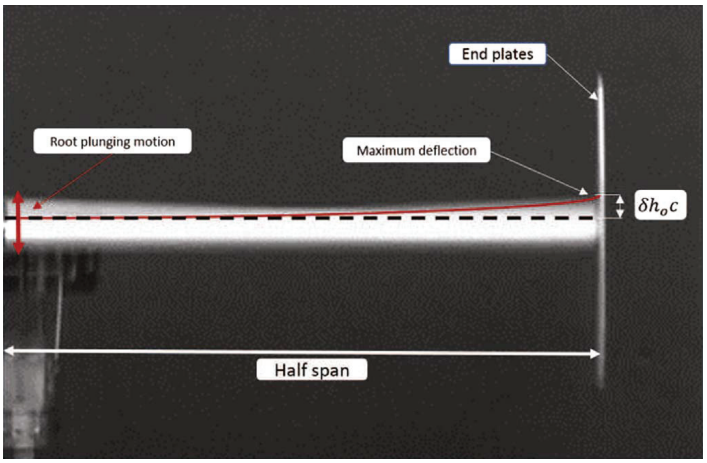

Fig. 5. High-speed photogrammetry image of the wing undergoing forced oscillatory motion at 18 Hz.

where m_{moving} is the mass of the moving parts, i.e. wing and oscillatory rods and the term $\pi\rho\ell b^2\cos^2\alpha$ is the theoretical prediction of the added mass (Yan et al., 2014), which is estimated to be about 0.012 kg in the case of $\alpha_o = 0°$. This estimate is the maximum value of the added mass force and constitutes only about 2.3% of the total mass. As such, any error in its estimation should not significantly impact the calculated circulatory lift coefficient. C_{Ls} is the quasi-steady lift defined by the instantaneous angle of attack and can be written as $C_{L_s}(t) = C_L(\alpha_{\text{eff}}(t))$, where the effective angle of attack is given by:

$$\alpha_{\text{eff}}(t) = \alpha_0 + \frac{\dot{h}(t)}{U_\infty} = \alpha_0 + \frac{2kh_a}{c}\cos(2\pi ft) \tag{4}$$

To ensure that the excitation frequency is far from the structure's natural frequency, we performed a free vibration test (strike-test), which showed that the first natural frequency is about 57 Hz. This frequency is much higher than the applied excitation frequencies that varied between 1.9 and 17.6 Hz. Furthermore, dynamic deformation measurements of the wing when excited at 18 Hz revealed a maximum deflection at the wing tip of about 0.3 cm, which is no more than 0.5% of the wing span, as shown in Fig. 5. As such, the wing's motion could be considered to be rigid.

4.1. Frequency response in the linear regime ($\alpha_0 = 0° - 10°$)

Fig. 6 shows time histories of the quasi steady lift coefficient C_{L_s}, the circulatory lift coefficient C_{L_c}, and the effective angle of attack α_{eff} along with the C_{L_s}-α_{eff} variations for $\alpha_0 = 0°$, 5° and 10° at selected value of the reduced frequency k. In all cases, the effective angle of attack lies within $\pm 5.7°$ of the mean angle of attack. For all cases shown, the effective angle of attack varies sinusoidally with a period equal to that of the plunging oscillations. Because the static lift coefficient varies linearly with the effective angle of attack, its time variations are also sinusoidal with one period. The circulatory lift also exhibits periodic variations with a period that is equal to that of the forced oscillations. Fig. 7 shows the obtained frequency responses along with Theodorsen's frequency response function for the cases of $\alpha_0 = 0°$, 5°, and 10°. The error bars show the extent of variation of the measured values from different data sets for each operating reduced frequency. Good agreement with Theodorsen's frequency response is noted over this range of mean angles of attack. This agreement is expected for small angles of attack and the no flow separation flat wake

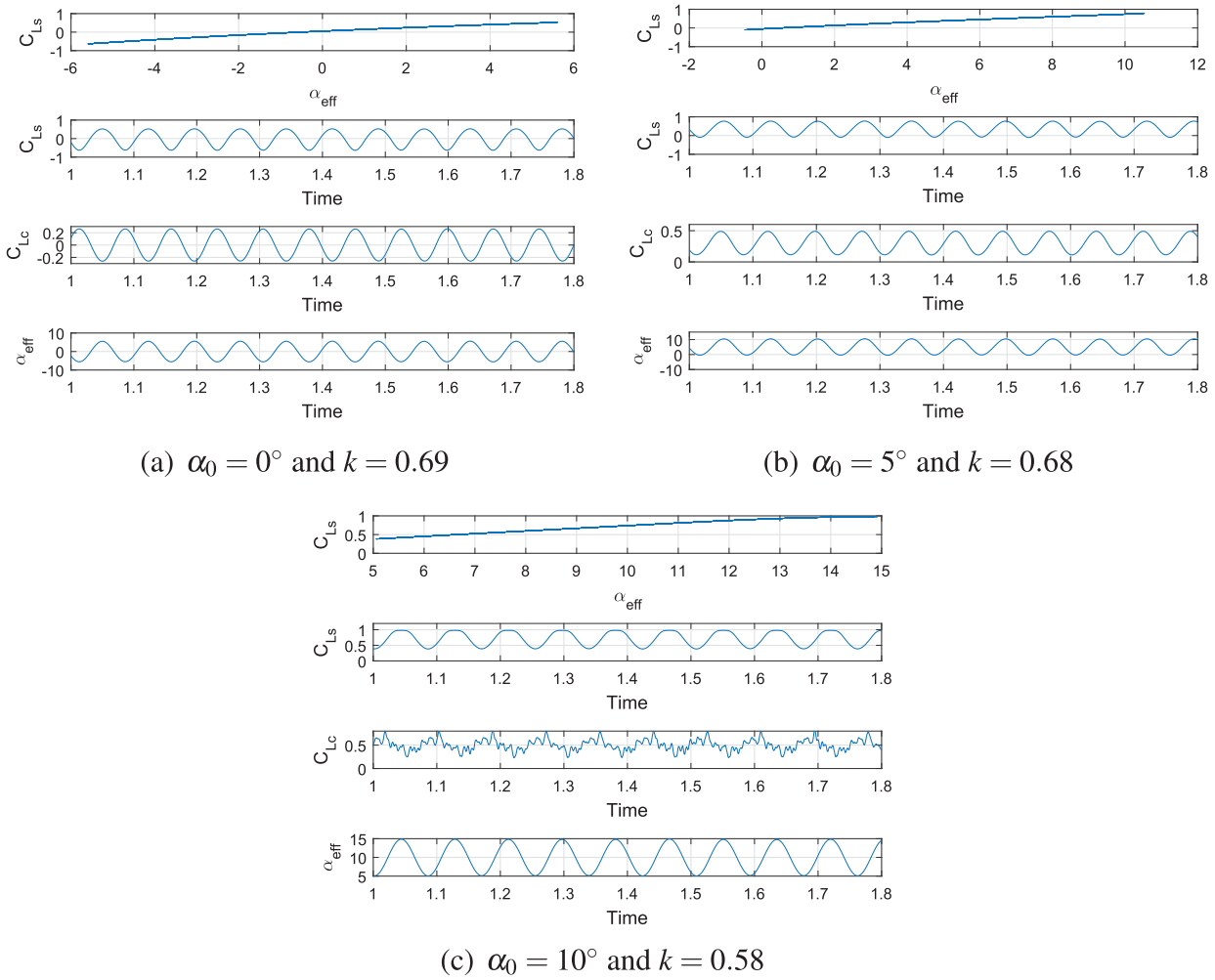

Fig. 6. Time histories of C_{L_s}, C_{L_c} and α_{eff} at various reduced frequencies along with the C_{L_s}-α_{eff} variation in the linear regime.

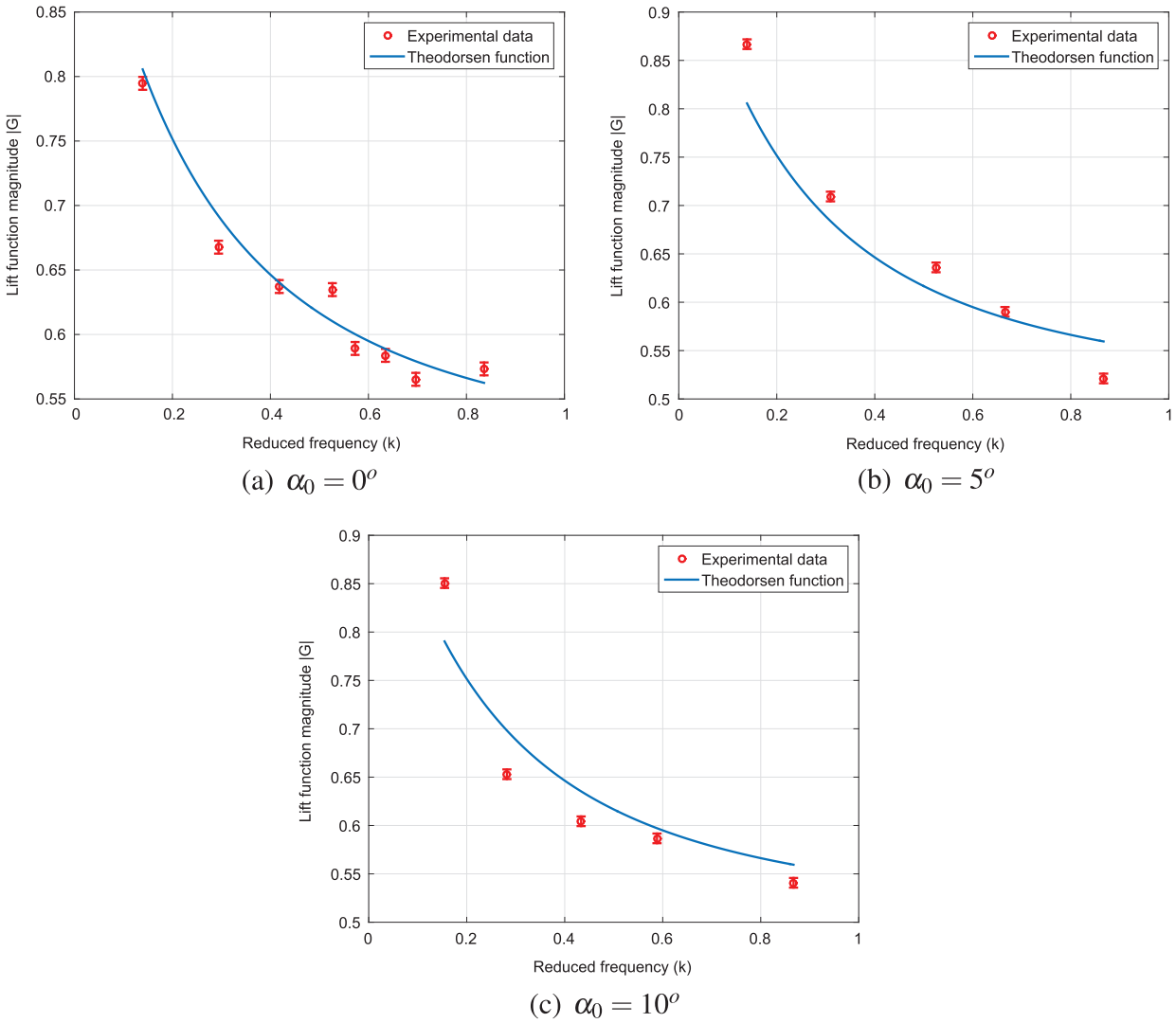

Fig. 7. Magnitude of the lift frequency response in the linear regime.

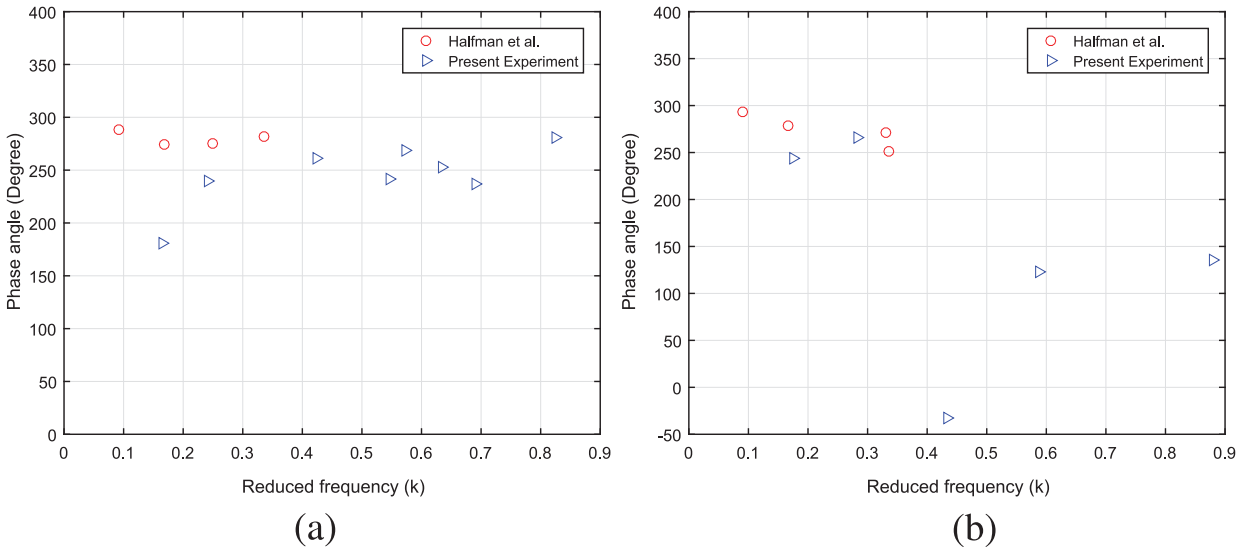

Fig. 8. Phase angle between the measured lift force and the plunging motion at (a) zero degree mean angle of attack, (b) 10° mean angle of attack. Current measurements and Halfman et al. (1951).

assumption is not severely violated. The obtained frequency response is monotonically decreasing as the frequency increases, which is similar to the response of a first-order simple lag system.

Analysis of the phase lag showed large variations, which has also been observed in the experimental measurements of Commerford and Carta (1974) who noted difficulties in accurate phase measurements, particularly at high-reduced frequencies. One reason for these variations could be the abundant chaotic vortex-wake interactions that occur at high Strouhal numbers as observed by Lentink et al. (2010). Even at zero mean angle of attack and low reduced frequencies, the experimental results of Halfman et al. (1951) showed significant deviations from Theodorsen's theoretical predictions. A comparison between the current measurements for the phase angle between the measured aerodynamic lift force and the applied plunging motion and that of Halfman et al. (1951)

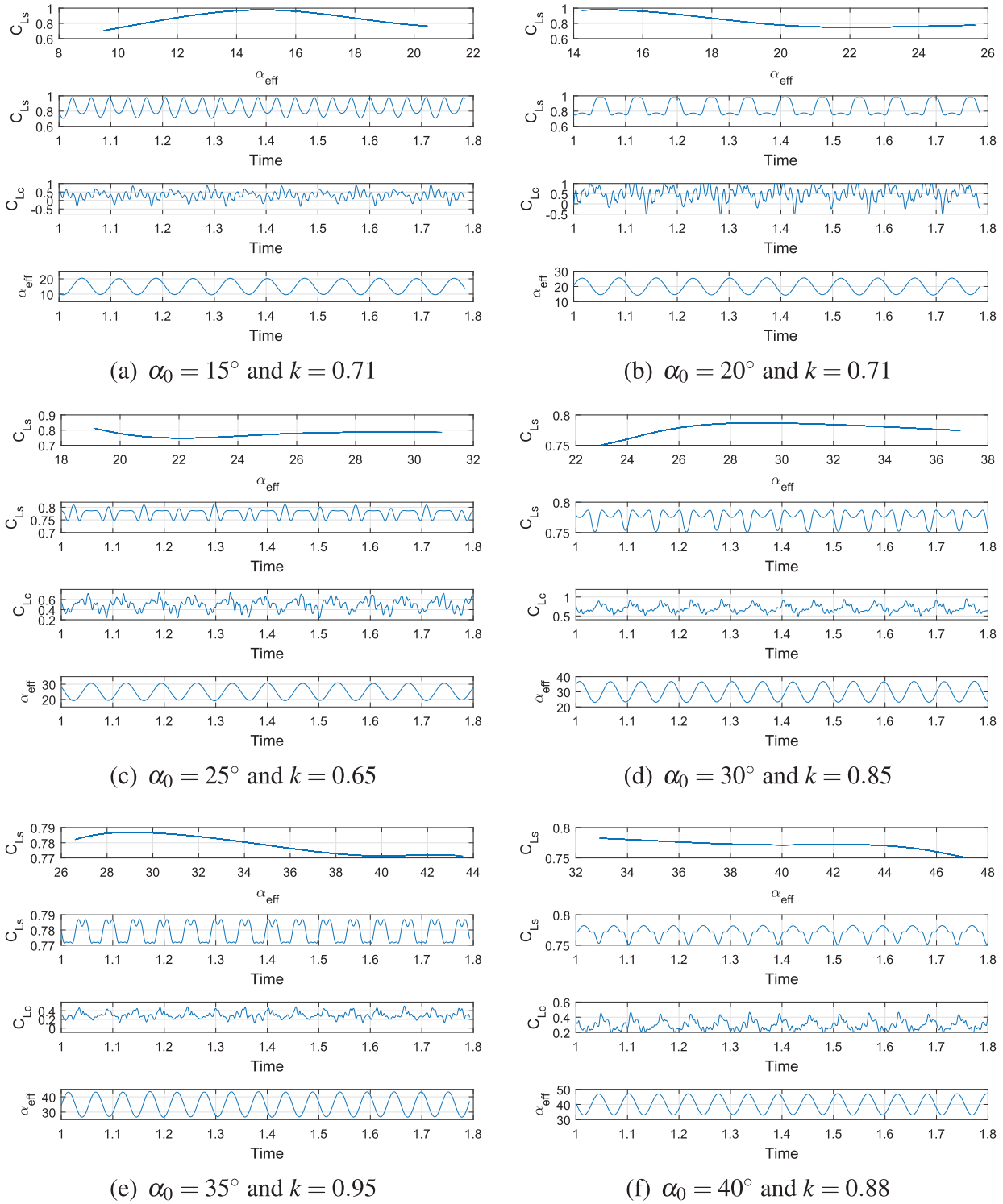

Fig. 9. Time histories of C_{Ls}, C_{Lc} and α_{eff} at various reduced frequencies along with the C_{Ls}-α_{eff} variation in the stall regime.

is presented in Figs. 8(a) and 8(b). Both sets of results differ slightly from theoretical predictions. It should be noted that Halfman's data does not include phase information at 14 degrees and beyond (16, 18, 20 and 22 degrees), because the resulting lift force is not periodic. In fact, at this moment, it is hard to assess whether the current phase measurements and Halfman's are, indeed, noisy or the classical unsteady theory fails to capture the phase accurately, as already suggested by several researchers (Bass et al., 1982;

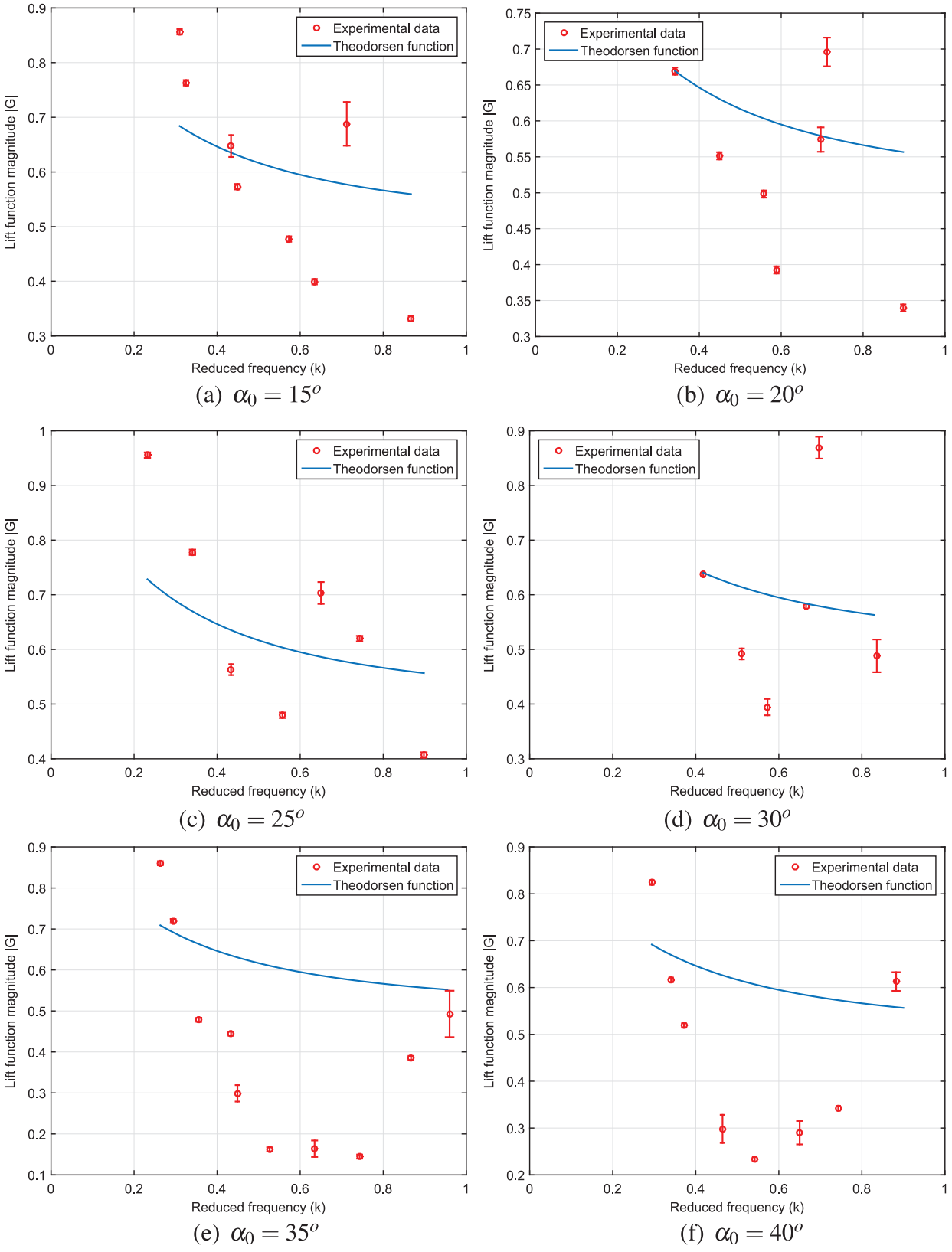

Fig. 10. Magnitude of the lift frequency response in the stall regime: α_0 varies between 15° and 40°.

Satyanarayana and Davis, 1977; Chu and Abramson, 1959).

4.2. Frequency response in the stall regime ($\alpha_0 = 15° - 40°$)

The frequency response in the stall regime cannot be predicted by Theodorsen's model. Even the model of Yan et al. (2014), though is geometrically valid for high angles of attack, presumed an attached flow and, hence, does not account for the effects of flow separation. Fig. 9 shows time histories of C_{Ls}, C_{Lc}, α_{eff}, and the C_{Ls}-α_{eff} variation over the range $15° \leq \alpha_0 \leq 40°$ for selected values of k.

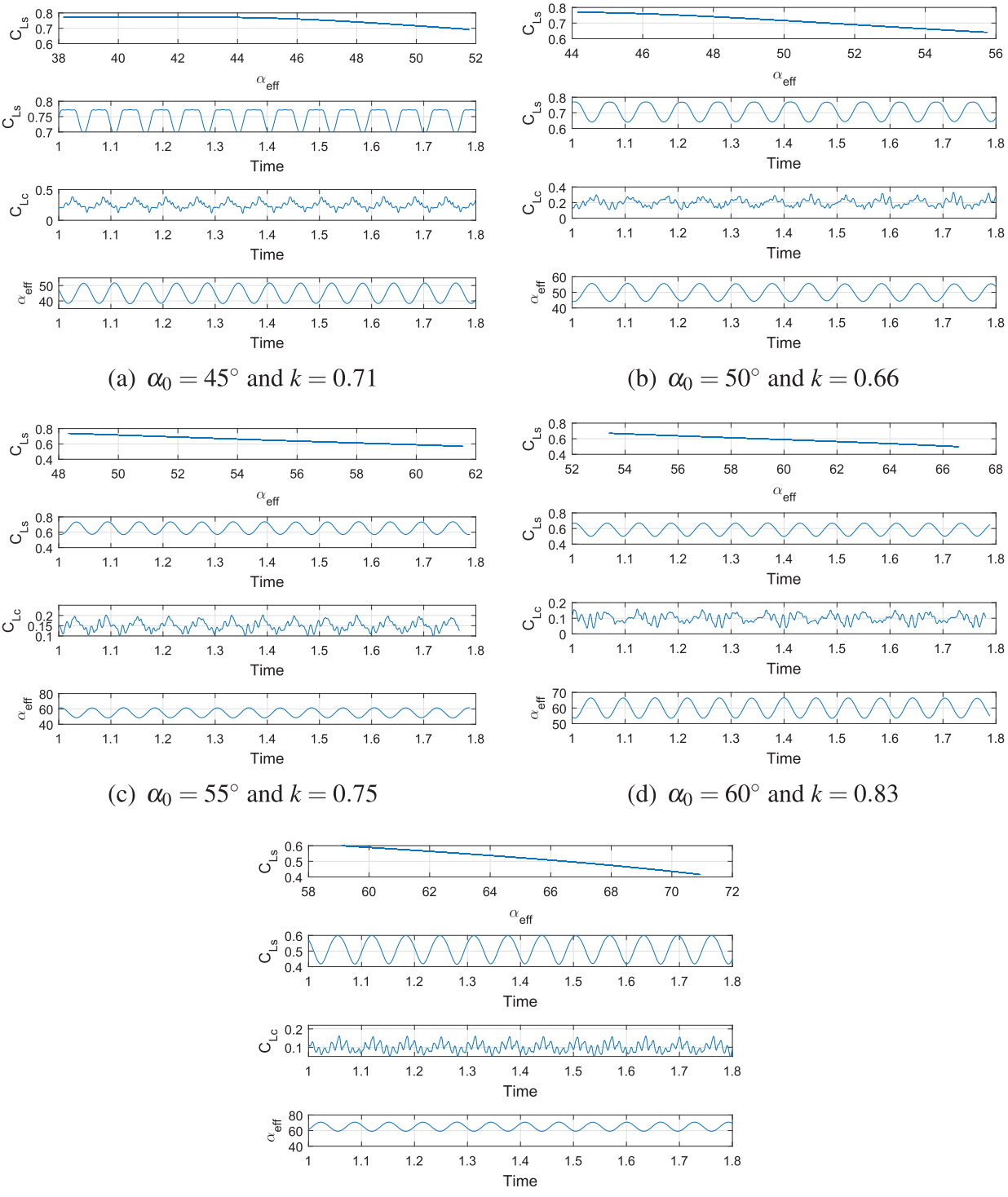

Fig. 11. Time histories of C_{Ls}, C_{Lc} and α_{eff} at various reduced frequencies along with the C_{Ls}-α_{eff} variation in the post-stall regime.

The nonlinearity of the static lift coefficient variation with the effective angle of attack is clearly shown. This nonlinearity can also be noted from the multi-frequency, periodic quasi-steady and circulatory lift coefficients although the wing oscillatory motion has a single frequency. Of particular importance is the appearance of superharmonics in the periodic variations of the static lift coefficients

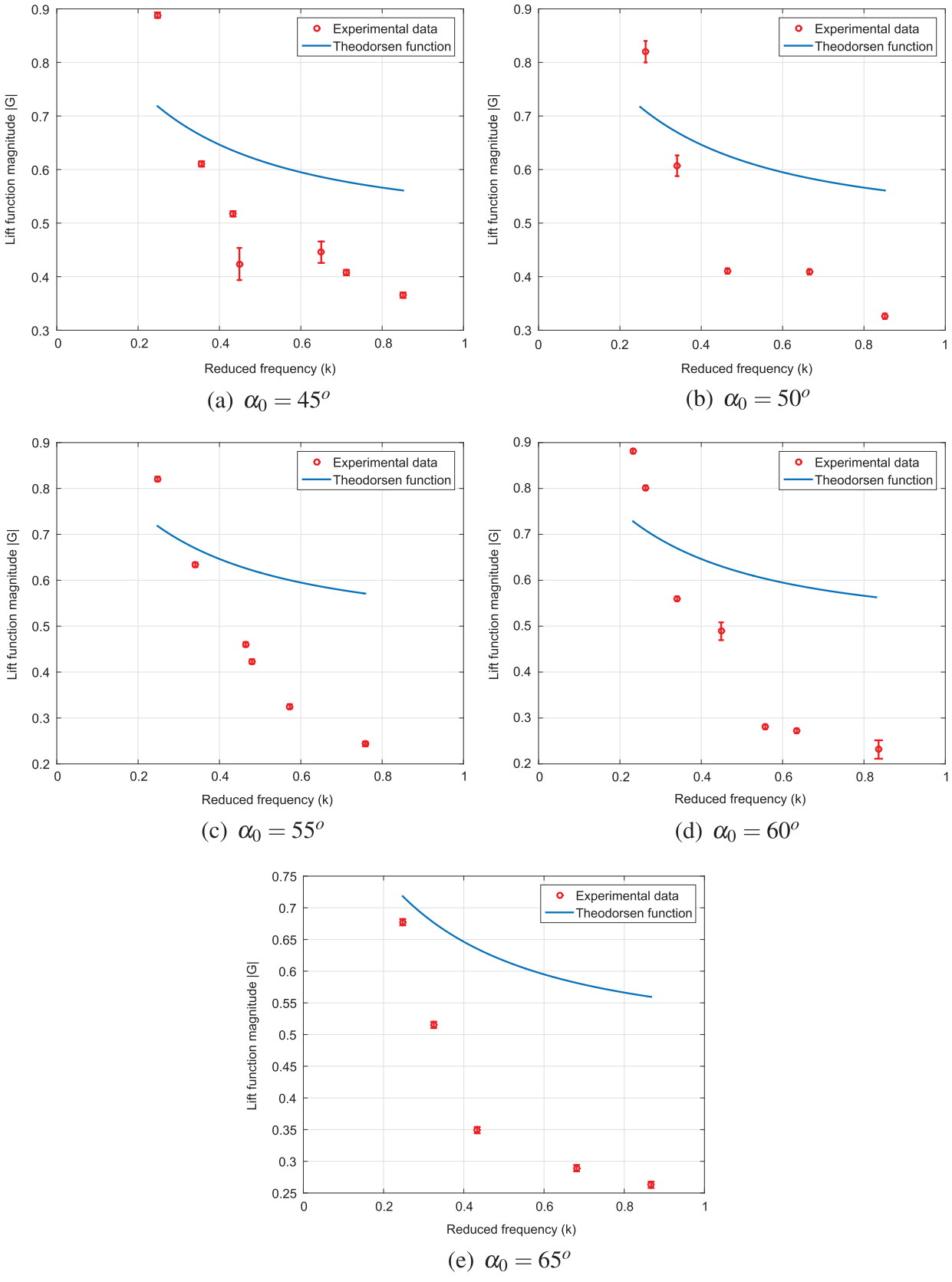

Fig. 12. Magnitude of the lift frequency response in the post-stall regime: α_0 varies between 45° and 60°.

that can be associated with the nonlinear variations of C_{Ls} with respect to α_{eff}. Furthermore, Figs. 9(a) and 9(b) show periodic variations in C_{Lc} value with many frequency components. We believe that these variations are due to a lock-in phenomenon occurs between different aspects of the flow dynamics even for fixed amplitude oscillations (Tang and Dowell, 2014) resulting from the plunging motion and/or vortex shedding.

Fig. 10 shows the magnitudes of the frequency response functions at $\alpha_0 = 15°$, 20°, 25° and 30° along with Theodorsen's. As expected, the obtained frequency responses in this regime are quite different from Theodorsen's; both qualitatively and quantitatively. Unlike the monotonically decreasing behavior of Theodorsen's frequency response, we note a decrease in the magnitude of the lift frequency response function as k increases up to values near 0.65–0.7. Around that value, we observe an increase in the magnitude of the frequency response, followed by a reduction as k is increased further. This finding is quite important for unsteady aerodynamics applications as it suggests significant enhanced lift generation around k=0.7. This value of reduced frequency corresponds to a Strouhal number based on the oscillation amplitude, h_a, S_{ta}=0.016 and a Strouhal number based on the chord, c, S_{tc}=0.23. The observed value of the lift-optimum frequency is consistent with the result obtained by Wang (2000). She used the Navier-Stokes equations to simulate impulsively started flow over a two dimensional wing section. She compared her numerical results to the experimental data of Dickinson and Gotz (1993). Both results show that the steady-state values of the lift cannot remain indefinitely constant at high angles of attack because of the well known LEV instability for two-dimensional flows (i.e., in the absence of a stabilizing axial or spanwise flows) and because a Von Karman street starts to emerge after about 10 chord lengths of travel. Wang (2000) concluded that there is a lift-optimum window for flapping that occurs after the steady state lift is reached, after the Wagner's lift transient behavior, and before the Von Karman oscillations start. We find that this window corresponds to a reduced frequency around k=0.7. Choi et al. (2015) used the immersed boundary method to perform a direct numerical simulation of Navier Stokes equations on a flat plate undergoing surging and plunging. The authors obtained a Fourier transform of the lift coefficient due to surging that is close to the potential flow theoretical prediction of Greenberg (1947) at small angles of attack (α = 5°). In addition, they found similar lift enhancement (lift amplitude) for surging airfoils over the same range of reduced

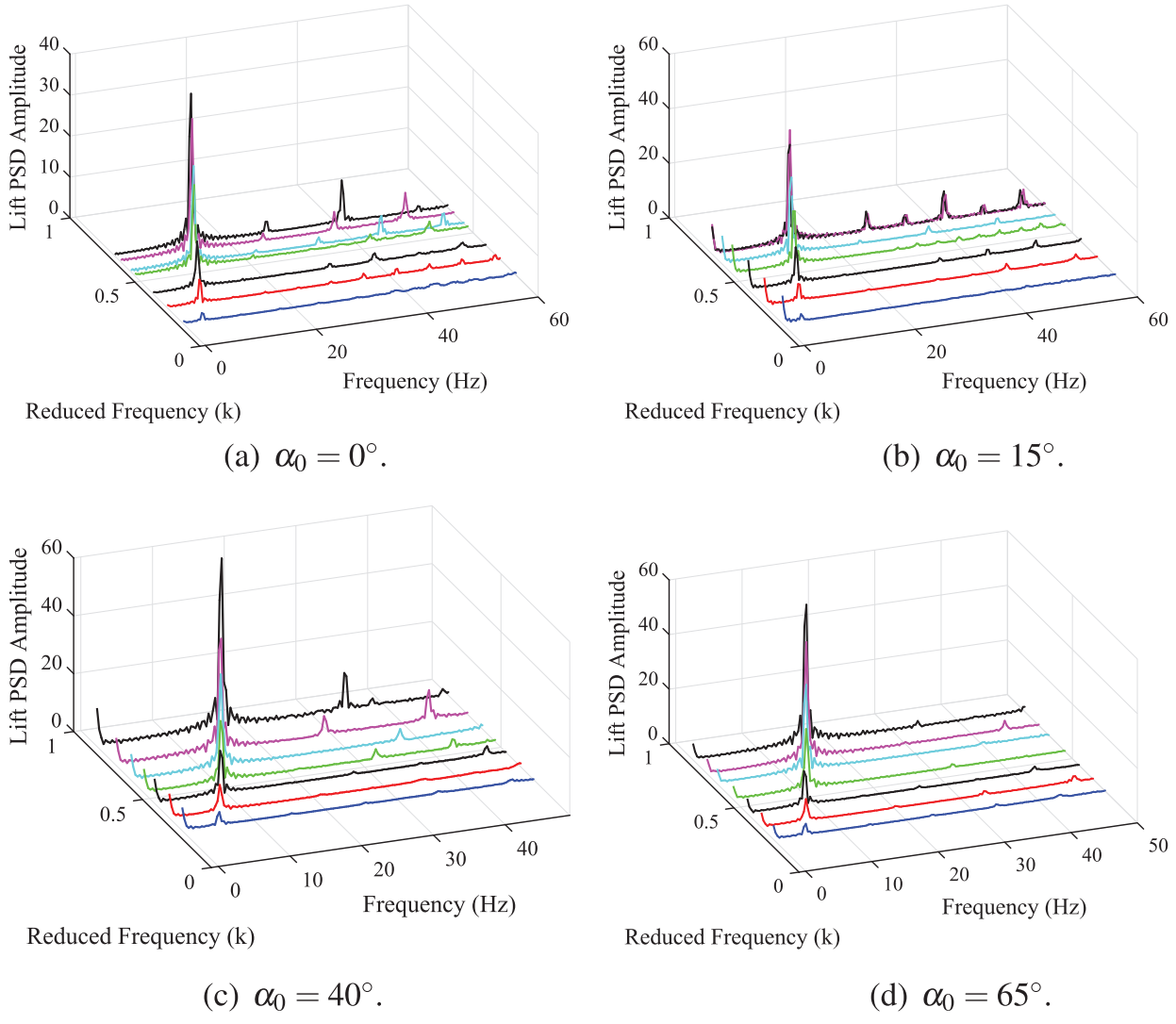

Fig. 13. Frequency spectra of the measured lift over NACA 0012 at *Re*=79,900 due to plunging at various reduced frequencies and mean angles of attack.

frequencies $k = 0.6 - 0.7$ at $\alpha = 15°$. The authors stated that airfoil plunging results in a similar behavior. Despite the difference in airfoil motion (pitch or plunge), motion frequency (reduced frequency k) and operating Reynolds number, a qualitative behavior of the observed lift enhancement mechanism is also consistent with the experimental findings of V. OL et al. (2009), Cleaver et al. (2013) and Calderon et al. (2013). Figs. 10(e) and 10(f) show the frequency response functions for $\alpha_0 = 35°$ and 40°, respectively. The plots show similar characteristics to the response functions obtained at lower angles of attack within the stall regime but with the lift-optimum frequency shifted to higher values. In fact, this shift can also be observed from the results of Choi et al. (2015) as their lift-peak frequency at Re=500 and 57,000 was k=0.6 at $\alpha = 15°$ and k=0.7 at $\alpha = 20°$. We consider the two cases of $\alpha_0 = 35°$ and 40° as a transition phase between stall and post-stall regimes.

4.3. Frequency response in the post-stall regime ($\alpha_0 = 45° - 65°$)

Fig. 11 shows time histories of C_{L_s}, C_{L_c}, α_{eff}, and the C_{L_s}-α_{eff} variation over the post-stall regime (i.e., $45° \leq \alpha_0 \leq 65°$). The results show a time response similar to that of the linear regime that is characterized by sinusoidal variations that have one period and an almost linear variation of C_{L_s} with α_{eff}. Fig. 12 shows the obtained frequency responses at $\alpha_0 = 45°$, 50°, 55°, 60°, and 65° along with that of Theodorsen's. The response functions regained their first-order-like behavior in this post-stall regime. As expected, Theodorsen's function does not agree with the measured values because the linear assumptions are not valid anymore. We also note the disappearance of the enhanced lift and the drop of the lift coefficient to values that are much smaller than values predicted by Theodorsen's function at high reduced frequencies. In agreement with the geometrically-exact potential flow theoretical predictions of Yan et al. (2014), the obtained magnitude of the lift frequency response in the post-stall regime is considerably smaller than that predicted by Theodorsen's, which can be satisfactorily attributed to flow separation from the leading edge.

4.4. Spectral analysis

Fig. 13 shows the frequency spectra of the measured lift due to plunging at various reduced frequencies, $0.15 \leq k \leq 0.95$, which corresponds to a frequency range between 1.9 and 17.6 Hz and mean angles of attack ($\alpha_0 = 0°$, 15°, 40°, and 65°). For all cases, a distinct peak is clearly noted at the excitation/forcing frequency. At α_0=0°, 15°, 40° and for $k < 0.6$, most of the energy of the lift fluctuations is concentrated in a frequency equal to that of the excitation frequency. For $k > 0.6$, we note the appearance of peaks at the superharmonics of the excitation frequency which is indicative of nonlinear interactions in flow dynamics. It should be noted that, the higher harmonics due to the nonlinear effects at relatively large reduced frequencies can be associated with the lift enhancement mechanism. Gursul et al. (2014) determined that this mechanism can be effective when the plunging frequency resonates with the natural shedding frequency, its harmonics or sub-harmonics. We will present below flow visualization to determine nonlinear flow characteristics including the formation and convection of the leading edge vortex that results in the enhanced lift. In the post-stall regime, spectra presented in Fig. 13(d) by α_0=65° show that the frequency components are not present, which indicates the reduced role or disappearance of the LEV.

5. Physical insight through flow visualization

In order to provide a physical insight into the observed lift enhancement mechanism, flow visualizations were performed by seeding ceramic particles in a water channel facility having a test chamber sectional area of 58 cm width and 83 cm height. The seeded particles were illuminated by a NDYAG laser sheet at the mid section of the used profile. High speed images were recorded at 200 frames per sec using a CCD camera with a resolution of 1024×840 pixels coupled with 50 mm f1.2 Nikon lens. The flow speed was 0.5 m/s, which yielded a Reynolds number of 70,000. The case of $k = 0.7$ was considered because it is the condition corresponding to the observed lift enhancement. The turbulence level is 1% and wing experienced less than $0.05c$ tip deflection due to hydrodynamic loading at the maximum operating frequency (1.2 Hz). Moreover the deflection is more negligible near the mid-span section where the visualization was performed. The advantage of using this technique versus a smoke visualization technique is that the generated streamlines would not deteriorate as they would at high flow speeds. The same pitch-plunge mechanism, wing profile (NACA 0012) and chord were used. The wing was painted with a matte black color to prevent reflection. The mechanism was suspended upside down above the test section as shown in Fig. 14.

Fig. 15 shows a flow visualization sequence of pictures taken over one period of pure plunging oscillation about $\alpha_0 = 15°$ at k=0.7.

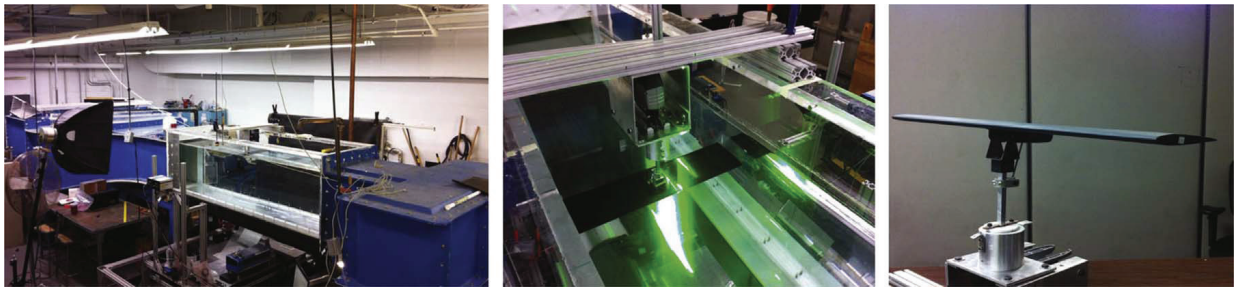

Fig. 14. Pitch-plunge mechanism mounted in the test chamber of the water channel.

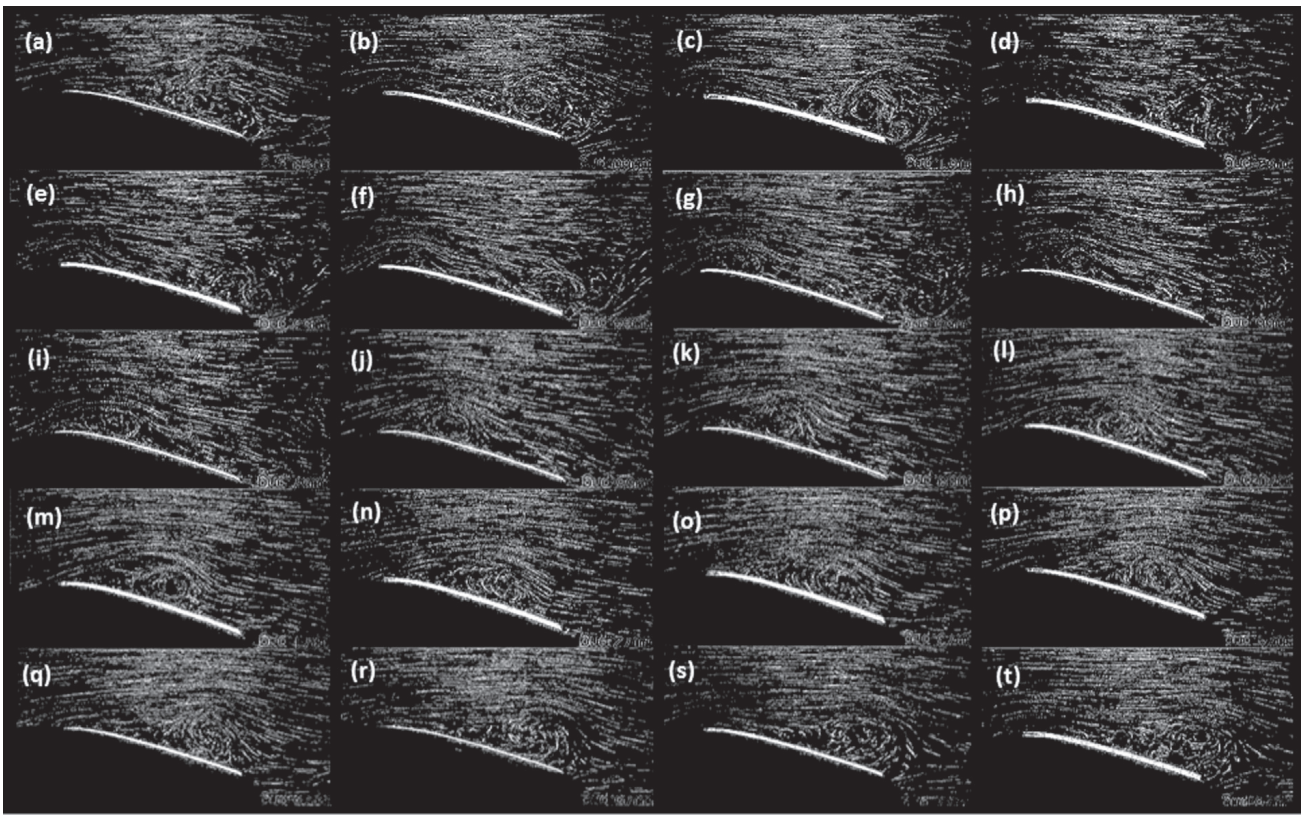

Fig. 15. Flow visualization sequence of one plunging period with k=0.7 at 15° AoA. The sequence starts at $t/T = 0$ (top of stroke (a)) and follows in constant steps of 1/20. The effective angle of attack varies between 9.5° and 20.5°.

The sequence starts at $t/T = 0$ with the wing at its highest position (*a*) and having zero velocity. It also shows pictures over constant time separations of $t/T = 1/20$. Because of the plunging velocity of the wing, the effective angle of attack varies between 20.5° at position (*f*) and 9.5° at position (*p*) (i.e., 15° ± 5.5°).

Between (*a*) and (*f*), the wing accelerates downwards from a zero plunging speed at (*a*) to a maximum plunging speed of 4.86 cm/s at (*f*), which corresponds to an increase in the effective angle of attack from 15° at (*a*) to 20.5° at (*f*). The vortex over the wing near the trailing edge, shown in (*a*), is a remnant of a LEV that has formed during the previous cycle. Between (*f*) and (*k*), the wing has a downward velocity while decelerating from 4.86 cm/s at (*f*) to zero velocity at (*k*). Consequently, the effective angle of attack decreases from 20.5 to 15°. This decrease results in the wing re-approaching the stall conditions. Over this time period, a LEV starts to form at position (*f*) and grows until it forms a coherent vortex structure at the (*j*) position. Between positions (*k*) and (*o*), the wing is moving upwards, which results in a further decrease in the effective angle of attack from 15° to 9.5°. Meanwhile, the LEV continues its excursion along the upper surface. Between (*o*) and (*t*), the wing moves upwards while decelerating, which results in an increase in α_{eff} from 9.5° to 15°. Over this region, the coherent structure becomes less visible indicating vortex breakdown as it leaves the trailing edge.

Fig. 16 shows a picture sequence from (*i*) to (*p*). On each picture, a cm ruler is placed along the airfoil chord to locate the position of the vortex core. Picture (*i*) shows the LEV at $0.3c$ from the leading edge. By tracing the picture sequence, one can observe a LEV

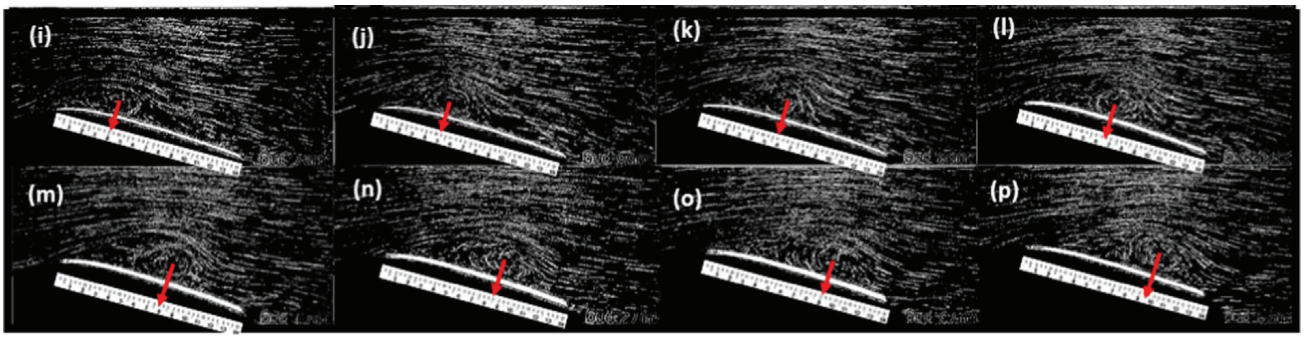

Fig. 16. Flow Visualization sequence pictures of the LEV convection on the upper surface of NACA 0012 listed in Fig. 15. A ruler placed along with the chord line is used to determine the vortex core.

convection velocity along the top surface of approximately 16 cm/s = $0.3U_\infty$. This relatively slow convection, in comparison to the free stream velocity, indicates that the LEV remains attached to the surface over this period. The presented visualization shows that the vortex forms when α_{eff} is close to 15° and the wing is moving downwards at a decelerating rate which mitigates separation effects. The wing deceleration allows the LEV to remain attached to the top surface. This synchronization between the reduction of the effective angle of attack and the development of the leading edge vortex results in lift enhancement. These observations are similar to those of Cleaver et al. (2011) who performed a plunging experiment at a mean angle of attack of 15° and lower Reynolds number (*Re*=10,000).

Li and Wu (2015) concluded that a LEV convecting downstream on the upper surface of an airfoil enhances the lift when it is near the leading edge and reduces the lift as it approaches the trailing edge. Inspecting Fig. 15, we find that, near the mid-stroke region covered by (*i*)-(*l*), the LEV maintains a strong core while convecting downstream on the upper surface and remaining close to the leading edge, which results in lift enhancement as suggested by Li and Wu (2015) and Chow et al. (1985). This LEV lift enhancement is coincident with the maximum quasi-steady lift at point (k) where $\alpha_{\text{eff}} = 15°$ as shown in Fig. 17. Likewise, near the maximum upward plunging speed covered by (*p*)-(*r*), the LEV approaches the trailing edge, causing a lift reduction that is also coincident with the lowest quasi-steady lift at point (*p*) where $\alpha_{\text{eff}} = 9.5°$. Therefore, similar to the conclusions of Choi et al. (2015), the observed lift enhancement mechanism is attributed to a synchronization between the motion frequency and LEV shedding time-scale such that the changes in the LEV lift and the quasi-steady lift are coincident.

To support the relation between flow dynamics and lift enhancement at *k*=0.7, we present in Fig. 18 a flow visualization comparison at reduced frequencies *k*=0.5, 0.7 and 0.9 at four stroke positions (top of the motion, mid-down, bottom and mid-up). The results at the wing top position (first column) in Fig. 18 show a clear remnant LEV in the case of *k*=0.5 and *k*=0.7 when compared to that of *k*=0.9. In particular, near the mid-stroke region (mid-down position) shown in second column, initiation of a LEV formation is observed at *k*=0.7 compared to cases of *k*=0.5 and *k*=0.9. Simultaneously, the maximum quasi-steady lift at zero plunging speed is attained. The formed LEV continues growing with a strong core structure for the case of *k*=0.7 compared to the weak formation at *k*=0.5. That is, there is no synchronization between the maximum quasi-steady lift and LEV lift in this case. Similarly, the fast excursion of the formed LEV for *k*=0.9 lead to a weak vortex structure. Additionally, the convection velocity of the LEV core is estimated to be $0.5U_\infty$ (i.e., 67% higher than that of the case of *k*=0.7). This relatively fast convection speed undermines the LEV lift. Moreover, near the maximum upward plunging speed (mid-up), a weak LEV is observed near the leading edge (i.e., a positive LEV lift). That is, there is a synchronization between the minimum quasi-steady lift and the maximum LEV lift; diminishing each other and resulting in an attenuation in the total lift amplitude (i.e., reduction in the lift frequency response).

6. Optimization based system identification

The flow dynamics in the linear regime can be satisfactorily described by Theodorsen's response. It should be noted that even the linearized, potential flow models (e.g., Theodorsen's and Wagner's) that also presume flat wake and shedding-by-free-stream result in infinite dimensional dynamical responses. To develop an efficient model that is suitable for optimization, sensitivity analysis, dynamics and control analyses as well as preliminary design of engineering systems, we seek a finite-dimensional approximation to the dynamical behavior (the frequency response) in each of the regimes discussed above. In fact, there is no consensus about the appropriate order of a finite-dimensional approximation even to a linear dynamical response. Useful two dimensional approximation for linear unsteady aerodynamics (i.e., Theodorsen's and Wagner's responses) were developed by Jones (1938) and Jones (1945).

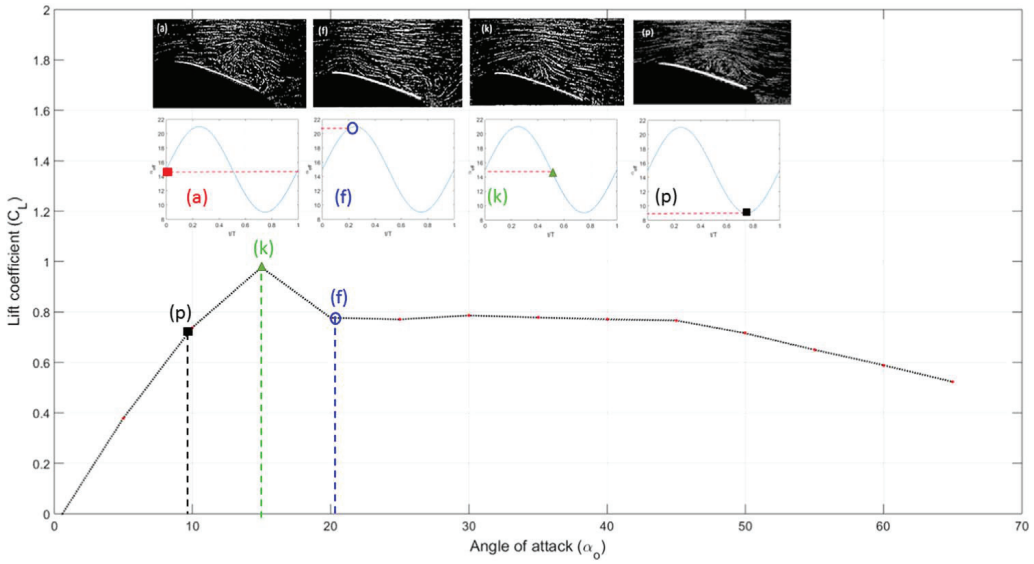

Fig. 17. Steady C_L-α curve of NACA 0012. The points marked corresponds to the effective angle of attack starting with the wing is at its highest position and going downward (*a*), at zero position and having a downward velocity (*f*), at the lowest position and going upward (*k*) and at zero position with an upward velocity (*p*).

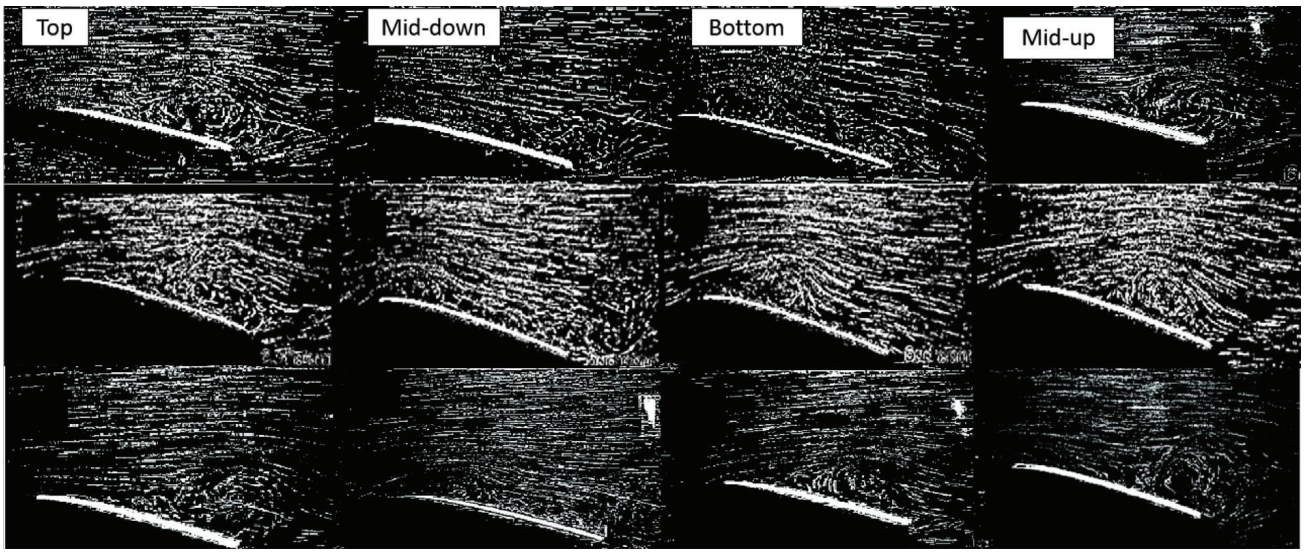

Fig. 18. Flow visualization sequence of one plunging period with k=0.5 (first row), k=0.7 (second row) and k=0.9 (third row) at 15° AoA. The sequence starts at $t/T = 0$ (top of stroke).

More recent work on finite-state aerodynamic modeling using Pade approximants can be found in Vepa (1976). In contrast to fitting Theodorsen's and Wagner's responses, finite-state models were derived from the basic principles by Peters and Karunamoorthy (1994), Peters et al. (1995), and Peters (2008), though required a relatively high order (eighth-order) for good accuracy. In this work, we proposed that the minimum order of a dynamical system that can fit the data of the stall-regime, which exhibited the most dynamically-rich response, is four. As such, we write the approximating fourth-order dynamical system as:

$$\frac{d}{d\tau}\begin{pmatrix}\chi_1(\tau)\\ \chi_2(\tau)\\ \chi_3(\tau)\\ \chi_4(\tau)\end{pmatrix}=\begin{bmatrix}0 & 1 & 0 & 0\\ 0 & 0 & 1 & 0\\ 0 & 0 & 0 & 1\\ -a_0 & -a_1 & -a_2 & -a_3\end{bmatrix}\begin{pmatrix}\chi_1(\tau)\\ \chi_2(\tau)\\ \chi_3(\tau)\\ \chi_4(\tau)\end{pmatrix}+\begin{pmatrix}0\\ 0\\ 0\\ 1\end{pmatrix}C_{L_s}(\alpha(\tau))C_{L_c}(\tau)=[b_0 \quad b_1 \quad b_2 \quad b_3]\begin{pmatrix}\chi_1(\tau)\\ \chi_2(\tau)\\ \chi_3(\tau)\\ \chi_4(\tau)\end{pmatrix} \tag{5}$$

where the χ's represent the internal aerodynamic states, $\tau=\frac{U_\infty t}{b}$ is the nondimensional time, and a's and b's are constant coefficients. The transfer function of the system (5) is written as:

$$G(p)=\frac{C_{L_c}(p)}{C_{L_s}(p)}=\frac{b_3p^3+b_2p^2+b_1p+b_0}{p^4+a_3p^3+a_2p^2+a_1p+a_0} \tag{6}$$

where, p is the non-dimensional Laplace variable corresponding to the non-dimensional time-variable τ. To obtain the magnitude of the frequency response of this transfer function, we substitute $p = ik$, which yields:

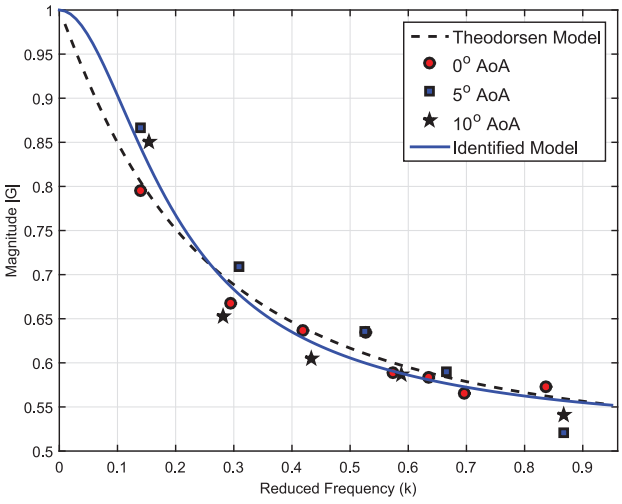

Fig. 19. Lift frequency response function for the linear regime (0–10° AOA).

$$|G(k)| = \sqrt{\frac{(b_0 - b_2\omega^2)^2 + (b_1\omega - b_3\omega^3)^2}{(a_0 - a_2\omega^2 + \omega^4)^2 + (a_1\omega - a_3\omega^3)^2}} \tag{7}$$

To determine the coefficients of the transfer function given in Eq. (6), we set up and solve, for each α_0, the following optimization problem.

$$\min_{\boldsymbol{x}} \quad e^2_{|G|} = \sum_{i}^{N} (|G(k_i)| - |G_{\text{meas}}(k_i)|)^2 \quad \text{subject to}$$

$$\frac{b_0}{a_0} = 1 \quad \text{and} \quad \mathcal{R}[\text{roots}(p^4 + a_3p^3 + a_2p^2 + a_1p + a_0)] < 0$$

where $\boldsymbol{x} = [a_0, a_1, a_2, a_3, b_0, b_1, b_2, b_3]$ represents the vector of design variables (transfer function coefficients), $|G_{\text{meas}}(k_i)|$ is the measured frequency response at the data point k_i, N is the number of measurements, and $\mathcal{R}$ represents the real part of its argument. The first (equality) constraint (i.e., unity transfer function dc gain) is dictated by the physics of the problem. That is, the ratio between the unsteady and steady loads at zero frequency must be unity. The second (inequality) constraint is to ensure that the selected transfer function given in Eq. (6) has poles with negative real parts; that is, we have stable flow dynamics as suggested by Jefferys et al. (1984). We use sequential quadratic programming to solve the above posed optimization problem. Fig. 19 shows the magnitude of the lift frequency response data points from the measurements at $\alpha_0 = 0°$, 5° and 10° along with that of Theodorsen's. Additionally, we show the frequency response of the fitted fourth-order system. The plot shows good matching among the three sets. It should be noted that the infinite dimensional nature of Theodorsen's response renders its magnitude an infinite slope at k=0, which cannot be realized by any finite-dimensional approximation. As such, there will always be a boundary-layer-like range near small values of k over which there is a mismatch between Theodorsen's response and its finite-dimensional approximation. On the other hand, because of Theodorsen's way of defining the circulatory lift, the high frequency gain is non-zero (1/2), which cannot be realized by any realistic dynamical system. A non-zero high-frequency gain comes from a transfer function whose numerator's degree is higher than or equal to its denominator's degree (i.e., non-strictly proper transfer function). This implies a non-zero instantaneous response of the system output. This non-physical behavior is due to Theodorsen's definition of the circulatory lift, which is the common definition in Fung (1995). Interestingly, the majority define the circulatory lift not as the lift due to bound circulation. Rather, they adopt an easily computed definition that incorporates an added-mass component. The former definition would result in an indicial response that has a zero initial value and a frequency response of a zero high-frequency gain. The latter common definition results in the Wagner's indicial response having initial value of 1/2 and the Thodorsen's frequency response having a high-frequency gain of 1/2. This point is discussed in detail in Peters (2008).

Theodorsen's model is based on a linear approximation for the flow dynamics, which results in a frequency response that is independent of the operating condition and/or the amplitude of the aerodynamic input (airfoil motion). However, the geometric and non-planar-wake nonlinearities are expected to result in a different frequency response (i.e., linearized flow dynamics) at different operating conditions (angles of attack). In addition, it is important to note that if an aeroelastic and/or flight dynamic stability is to be checked around some equilibrium at relatively large angle of attack (i.e., $\alpha > 10°$), Theodorsen's linear model will not be valid even for the sake of linear/local stability analysis. This motivates developing even a linearized model governing the flow dynamics at high angle of attack. Fig. 20 shows the three sets of frequency response data including the measured points, Theodorsen's response and the fitted fourth-order representations for $\alpha_0 = 15°$, 20°, 25° and 30°. The results show that the proposed fourth order model is able to capture the flow dynamics in the stall regime. Since the frequency responses at $\alpha_0 = 35°$ and 40° are different from that of the whole stall regime (lift enhancement shifted towards higher reduced frequencies), we did not consider their data in the optimization process for the stall regime. As mentioned earlier, we consider these cases as a transition phase between stall and post-stall regimes.

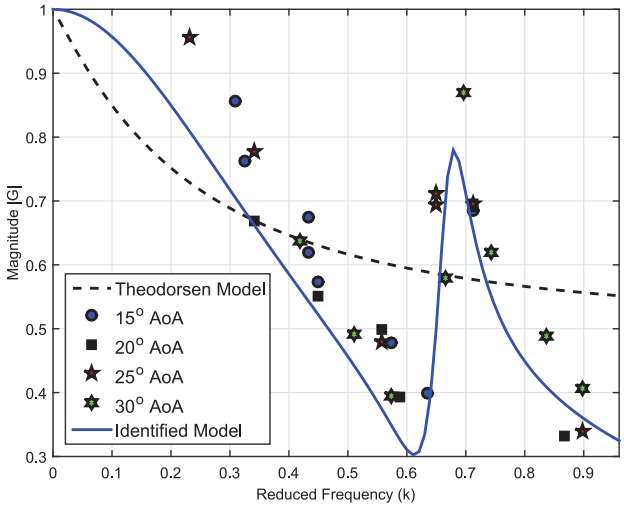

Fig. 20. Lift frequency response function for the stall regime (15–30° AOA).

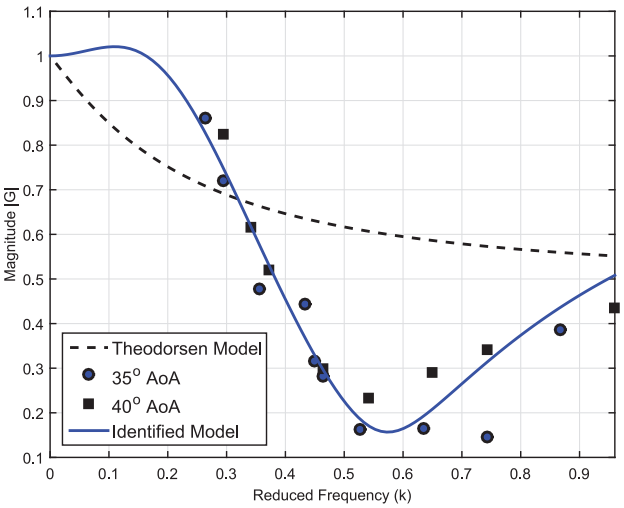

Fig. 21. Lift frequency response function for the transition regime between stall and post-stall ($30° < \alpha < 45°$).

To complete the reduced-order model, we followed the same optimization procedure to model this transition phase, as shown in Fig. 21.

Fig. 22 shows the three sets of frequency response data for $\alpha_0 = 45°, 50°, 55°, 60°$ and 65°. The results show good matching between the proposed model and the experimental data for all operating angles of attack.

Although the conducted experiment and the developed model were using NACA 0012, it is envisaged that the developed reduced-order model can capture the flow dynamics for other airfoil geometries including asymmetric airfoils. This expectation stems from the facts that (i) the main physics of unsteady flow dynamics is not considerably affected by airfoil geometry and (ii) can be represented by sustaining the operating Reynolds number along with sharp leading edge. In addition this conclusion is consistent with the finding of OL et al. (2009), where the former found that flowfields for the tested SD7003 airfoil and flat plate at reduced frequency of k=0.7 are reasonably similar assuming that motion-induced effects dominate those of the model cross-section.

7. Conclusions

Experiments on a two-dimensional NACA 0012 undergoing plunging oscillations in a wind tunnel at a Reynolds number of 80,000 were conducted to determine and model an operational range over which lift enhancement is observed. The plunging oscillations were performed at various mean angles of attack between 0° and 65° and reduced frequencies between 0.15 and 0.95. For different combinations of mean angles of attack and reduced frequencies, the lift time-history was measured along with the wing plunging acceleration. The acceleration was used to estimate the inertial and added mass loads and, therefore, extract the circulatory lift from the measured lift forces. In addition, the measured plunging acceleration was integrated to determine the plunging velocity and, consequently, the effective angle of attack. As such, the quasi-steady lift was calculated from measured steady lift characteristics. Then, the frequency response, defined as the ratio between the circulatory lift and the quasi-steady lift was constructed for each mean angle of attack. The results show that, in the linear range (0–10°), the obtained frequency responses

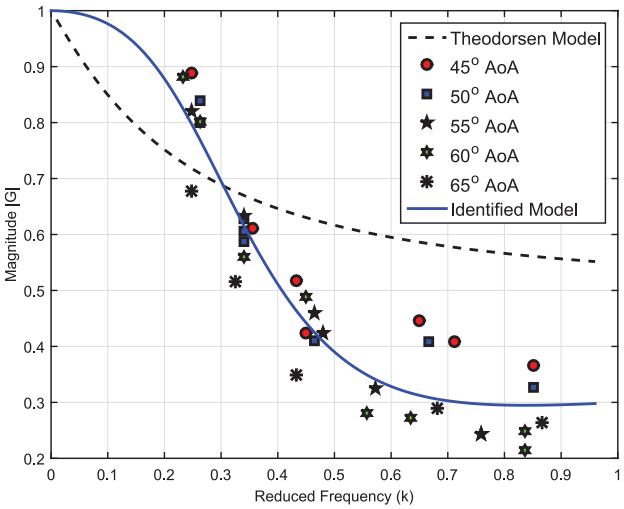

Fig. 22. Lift frequency response function for the post-stall regime (45–65° AOA).

match the classical Theodorsen's frequency response function. In the stall regime between 15° and 40°, the time series of the lift coefficients exhibit more than one period, though the airfoil motion has one period, which indicated significant nonlinear effects and departure from Theodorsen's frequency response. Particularly, the obtained frequency response exhibited a peak near a reduced frequency of 0.7. In the post-stall regime, the obtained frequency response regains its monotonically decreasing (first-order-type) dynamical nature with much smaller lift amplitude than that of Theodorsen's. To explain the basis of the observed lift enhancement mechanism in the stall regime near k=0.7, we performed flow visualization in a water channel. The visualizations show a leading edge vortex that forms and remains attached to the upper surface of the airfoil before moving downstream as the effective angle of attack is changed. Finally, an optimization-based fourth-order dynamical model was developed to match the obtained frequency responses at each mean angle of attack. These developed reduced-order dynamical models are quite suitable for sensitivity and control design applications for large amplitude maneuvers where unsteady aerodynamics can be exploited for the purpose of lift enhancement.

Acknowledgements

The authors would like to acknowledge the NSF grant CMMI-1635673.

References

Anderson, J., Streitlien, K., Barrett, D., Triantafyllou, M., 1998. Oscillating foils of high propulsive efficiency. J. Fluid Mech. 360 (1), 41–72.
Ansari, S.A., Żbikowski, R., Knowles, K., 2006. Non-linear unsteady aerodynamic model for insect-like flapping wings in the hover. Part 1: methodology and analysis. Proc. Inst. Mech. Eng. Part G: J. Aerosp. Eng. 220 (2), 61–83.
Baik, Y.S., Bernal, L.P., Granlund, K., Ol, M.V., 2012. Unsteady force generation and vortex dynamics of pitching and plunging aerofoils. J. Fluid Mech. 709, 37–68.
Bass, R., Johnson, J., Unruh, J., 1982. Correlation of lift and boundary-layer activity on an oscillating lifting surface. AIAA J. 20 (8), 1051–1056.
Berman, G.J., Wang, Z.J., 2007. Energy-minimizing kinematics in hovering insect flight. J. Fluid Mech. 582 (1), 153–168.
Birnbaum, W., 1924. Der schlagflugelpropeller und die kleinen schwingungen elastisch befestigter tragfluegel. In: Z Flugtech Motorluftschiffahrt, vol. 15, pp. 128–134.
Brooks, T.F., Marcolini, M.A., Pope, D.S., 1984. Airfoil trailing edge flow measurements and comparison with theory incorporating open wind tunnel corrections. AIAA Pap., 84–2266.
Brunton, S.L., Rowley, C.W., 2013. Empirical state-space representations for theodorsens lift model. J. Fluids Struct. 38, 174–186.
Calderon, D., Wang, Z., Gursul, I., 2013. Lift-enhancing vortex flows generated by plunging rectangular wings with small amplitude. AIAA J. 51 (12), 2953–2964.
Choi, J., Colonius, T., Williams, D.R., 2015. Surging and plunging oscillations of an airfoil at low reynolds number. J. Fluid Mech. 763, 237–253.
Chow, C.-Y., Huang, M.-K., Yan, C.-Z., 1985. Unsteady flow about a joukowski airfoil in the presence of moving vortices. AIAA J. 23 (5), 657–658.
Chu, W.-h., Abramson, H., 1959. Hydrodynamic theories of ship slamming: review and extension. Technical report.
Cleaver, D., Wang, Z., Gursul, I., 2013. Investigation of high-lift mechanisms for a flat-plate airfoil undergoing small-amplitude plunging oscillations. AIAA J. 51 (4), 968–980.
Cleaver, D.J., Wang, Z., Gursul, I., 2012. Bifurcating flows of plunging aerofoils at high strouhal numbers. J. Fluid Mech. 708, 349–376.
Cleaver, D.J., Wang, Z., Gursul, I., Visbal, M., 2011. Lift enhancement by means of small-amplitude airfoil oscillations at low reynolds numbers. AIAA J. 49 (9), 2018–2033.
Commerford, G., Carta, F., 1974. Unsteady aerodynamic response of a two-dimensional airfoil at high reduced frequency. AIAA J. 12 (1), 43–48.
Dickinson, M.H., Gotz, K.C., 1993. Unsteady aerodynamic performance of model wings at low reynolds numbers. J. Exp. Biol. 174 (1), 45–64.
Dickinson, M.H., Lehmann, F.-O., Sane, S.P., 1999. Wing rotation and the aerodynamic basis of insect flight. Science 284 (5422), 1954–1960.
Eldredge, J.D., Wang, C., Ol, M.V., 2009. A computational study of a canonical pitch-up, pitch-down wing maneuver. AIAA Pap., 2009–3687.
Ellington, C.P., Van Den Berg, C., Willmott, A.P., Thomas, A.L.R., 1996b. Leading-edge vortices in insect flight. Nature 384, 626–630.
Ellington, C.P., Van Den Berg, C., Willmott, A.P., Thomas, A.L., 1996a. Leading-edge vortices in insect flight.
Fung, Y.-C., 1995. An introduction to the theory of aeroelasticity. Courier Corporation.
Garner, H.C., Rogers, E., Acum, W., Maskell, E., 1966. Subsonic wind tunnel wall corrections. Technical Report, DTIC Document.
Graftieaux, L., Michard, M., Grosjean, N., 2001. Combining piv, pod and vortex identification algorithms for the study of unsteady turbulent swirling flows. Meas. Sci. Technol. 12 (9), 1422.
Greenberg, J.M., 1947. Airfoil in sinusoidal motion in a pulsating stream. Technical Report, NACA.
Gursul, I., Cleaver, D., Wang, Z., 2014. Control of low reynolds number flows by means of fluid-structure interactions. Prog. Aerosp. Sci. 64, 17–55.
Halfman, R.L., Johnson, H., Haley, S., 1951. Evaluation of high-angle-of-attack aerodynamic-derivative data and stall-flutter prediction techniques. Technical Report, DTIC Document.
Heathcote, S., Gursul, I., 2007. Jet switching phenomenon for a periodically plunging airfoil. Phys. Fluids 19 (2), 027104, (1994-Present).
Hemati, M.S., Eldredge, J.D., Speyer, J.L., 2014. Improving vortex models via optimal control theory. J. Fluids Struct. 49, 91–111.
Jefferys, E., Broome, D., Patel, M., 1984. A transfer function method of modeling systems with frequency-dependent coefficients. J. Guid. Control Dyn. 7 (4), 490–494.
Jones, K., Dohring, C., Platzer, M., 1996. Wake structures behind plunging airfoils: a comparison of numerical and experimental results. AIAA Pap. 78, 1996.
Jones, M.A., 2003. The separated flow of an inviscid fluid around a moving flat plate. J. Fluid Mech. 496, 405–441.
Jones, R.T., 1938. Operational treatment of the nonuniform lift theory to airplane dynamics. Technical Report 667, NACA.
Jones, W.P., 1945. Aerodynamic forces on wings in non-uniform motion. Technical Report 2117, British Aeronautical Research Council.
Leishman, J.G., Nguyen, k.Q., 1990. State-space representation of unsteady airfoil behavior. AIAA J. 28 (5), 836–844.
Lentink, D., Van Heijst, G.F., Muijres, F.T., Van Leeuwen, J.L., 2010. Vortex interactions with flapping wings and fins can be unpredictable. Biol. Lett., (rsbl20090806).
Li, J., Wu, Z.-N., 2015. Unsteady lift for the wagner problem in the presence of additional leading/trailing edge vortices. J. Fluid Mech. 769, 182–217.
Mangler, W., 1938. The lift distibution of wings with end plates. Technical Report, Technical Memorandum NASA TM 856, NASA.
Minotti, F.O., 2002. Unsteady two-dimensional theory of a flapping wing. Phys. Rev. E 66 (5), 051907.
Moffat, R.J., 1985. Using uncertainty analysis in the planning of an experiment. J. Fluids Eng. 107 (2), 173–178.
Ohmi, K., Coutanceau, M., Daube, O., Loc, T.P., 1991. Further experiments on vortex formation around an oscillating and translating airfoil at large incidences. J. Fluid Mech. 225, 607–630.
Panah, A.E., Buchholz, J.H., 2014. Parameter dependence of vortex interactions on a two-dimensional plunging plate. Exp. Fluids 55 (3), 1–19.
Peters, D.A., 2008. Two-dimensional incompressible unsteady airfoil theoryan overview. J. Fluids Struct. 24, 295–312.
Peters, D.A., Karunamoorthy, S., Cao, W., 1995. Finite-state induced flow models part i two-dimensional thin airfoil. J. Aircr. 44, 1–28.
Peters, D.A., Karunamoorthy, S., 1994. State-space inflow models for rotor aeroelasticity. AIAA-Paper 94-1920-CP.
Pitt Ford, C., Babinsky, H., 2013. Lift and the leading-edge vortex. J. Fluid Mech. 720, 280–313.

Polhamus, E.C., 1966. A concept of the vortex lift of sharp-edge delta wings based on a leading-edge-suction analogy. Technical Report NASA TN D-3767, Langely Research Center, Langely Station, Hampton, Va.
Prandtl, L., 1924. Über die entstehung von wirbeln in der idealen flüssigkeit, mit anwendung auf die tragflügeltheorie und andere aufgaben. In: Vorträge aus dem Gebiete der Hydro-und Aerodynamik (Innsbruck 1922), Springer, pp. 18–33.
Pullin, D.I., Wang, Z., 2004. Unsteady forces on an accelerating plate and application to hovering insect flight. J. Fluid Mech. 509, 1–21.
Rae, W.H., Pope, A., 1984. Low-Speed Wind Tunnel Testing. John Wiley.
Ramamurti, R., Sandberg, W., 2002. A three-dimensional computational study of the aerodynamic mechanisms of insect flight. J. Exp. Biol. 205 (10), 1507–1518.
Ramesh, K., Murua, J., Gopalarathnam, A., 2015. Limit-cycle oscillations in unsteady flows dominated by intermittent leading-edge vortex shedding. J. Fluids Struct. 55, 84–105.
Ramesh, K., Gopalarathnam, A., Edwards, J.R., Ol, M.V., Granlund, K., 2013. An unsteady airfoil theory applied to pitching motions validated against experiment and computation. Theor. Comput. Fluid Dyn., 1–22.
Ramesh, K., Gopalarathnam, A., Granlund, K., Ol, M.V., Edwards, J.R., 2014. Discrete-vortex method with novel shedding criterion for unsteady aerofoil flows with intermittent leading-edge vortex shedding. J. Fluid Mech. 751, 500–538.
Rival, D., Tropea, C., 2010. Characteristics of pitching and plunging airfoils under dynamic-stall conditions. J. Aircr. 47 (1), 80–86.
Rival, D.E., Kriegseis, J., Schaub, P., Widmann, A., Tropea, C., 2014. Characteristic length scales for vortex detachment on plunging profiles with varying leading-edge geometry. Exp. Fluids 55 (1), 1–8.
Saffman, P.G., Sheffield, J.S., 1977. Flow over a wing with an attached free vortex. Stud. Appl. Math. 57, 107–117.
Satyanarayana, B., Davis, S., 1977. Experimental studies of trailing-edge conditions on an oscillating airfoil at frequency parameters of up to one.
Savage, S.B., Newman, B.G., Wong, D.T.-M., 1979. The role of vortices and unsteady effects during the hovering flight of dragonflies. J. Exp. Biol. 83 (1), 59–77.
Sun, M., Du, G., 2003. Lift and power requirements of hovering insect flight. Acta Mech. Sin. 19 (5), 458–469.
Taha, H.E., Hajj, M.R., Beran, P.S., 2014. State space representation of the unsteady aerodynamics of flapping flight. Aerosp. Sci. Technol. 34, 1–11.
Taha, H.E., Yan, Z., Hajj, M.R., 2015. Geometrically-exact extension of theodorsen's frequency response model. In: Proceedings of the 53rd AIAA Aerospace Sciences Meeting 5–9 January 2015, Kissimmee, Florida, number AIAA-Paper 2015–1707.
Tang, D., Dowell, E.H., 2014. Experimental aerodynamic response for an oscillating airfoil in buffeting flow. AIAA J. 52 (6), 1170–1179.
Theodorsen, T., 1935. General theory of aerodynamic instability and the mechanism of flutter. Technical Report 496, NACA.
Triantafyllou, G., Triantafyllou, M., Grosenbaugh, M., 1993. Optimal thrust development in oscillating foils with application to fish propulsion. J. Fluids Struct. 7 (2), 205–224.
Usherwood, J.R., Ellington, C.P., 2002. The aerodynamics of revolving wings i. model hawkmoth wings. J. Exp. Biol. 205, 1547–1564.
V. OL, M., Eldredge, J.D., Wang, C., 2009. High-amplitude pitch of a flat plate: an abstraction of perching and flapping. Int. J. Micro Air Veh. 1 (3), 203–216.
Vepa, R., 1976. On the use of pade approximants to represent unsteady aerodynamic loads for arbitrarily small motions of wings. Washington, DC. AIAA, In: Proceedings of the 14th Aerospace Sciences Meeting, pp. 7–17.
Wagner, H., 1925. Uber die entstehung des dynamischen auftriebes von traflgugeln. Z. Angew. Math. Mech. 35, 17.
Wang, C., Eldredge, J.D., 2012. Low-order phenomenological modeling of leading-edge vortex formation. Theor. Comput. Fluid Dyn., 1–22.
Wang, Z., 2000. Vortex shedding and frequency selection in flapping flight. J. Fluid Mech. 410, 323–341.
Wang, Z.J., 2005. Dissecting insect flight. Annu. Rev. Fluid Mech. 37, 183–210.
Yan, Z., Taha, H.E., Hajj, M.R., 2014. Geometrically-exact unsteady model for airfoils undergoing large amplitude maneuvers. Aerosp. Sci. Technol. 39, 293–306.
Yongliang, Y., Binggang, T., Huiyang, M., 2003. An analytic approach to theoretical modeling of highly unsteady viscous flow excited by wing flapping in small insects. Acta Mech. Sin. 19 (6), 508–516.
Zakaria, M.Y., Al-Haik, M.Y., Hajj, M.R., 2015a. Experimental analysis of energy harvesting from self-induced flutter of a composite beam. Appl. Phys. Lett. 107 (2), 023901.
Zakaria, M.Y., Taha, H.E., Hajj, M.R., 2015b. Design optimization of flapping ornithopters: the pterosaur replica in forward flight. J. Aircr.. http://dx.doi.org/10.2514/1.C033154.